The *Drosophila* spectraplakin Short stop regulates focal adhesion dynamics by cross-linking microtubules and actin

Andrew J. Zhao[a,†], Julia Montes-Laing[a,†], Wick M.G. Perry[a], Mari Shiratori[a], Emily Merfeld[a], Stephen L. Rogers[b], and Derek A. Applewhite[a,*]

[a]Department of Biology, Reed College, Portland, OR 97202; [b]Department of Biology and Carolina Center for Genome Sciences, The University of North Carolina at Chapel Hill, Chapel Hill, NC 27599-3280

ABSTRACT The spectraplakin family of proteins includes ACF7/MACF1 and BPAG1/dystonin in mammals, VAB-10 in *Caenorhabditis elegans, Magellan* in zebrafish, and Short stop (Shot), the sole *Drosophila* member. Spectraplakins are giant cytoskeletal proteins that cross-link actin, microtubules, and intermediate filaments, coordinating the activity of the entire cytoskeleton. We examined the role of Shot during cell migration using two systems: the in vitro migration of *Drosophila* tissue culture cells and in vivo through border cell migration. RNA interference (RNAi) depletion of Shot increases the rate of random cell migration in *Drosophila* tissue culture cells as well as the rate of wound closure during scratch-wound assays. This increase in cell migration prompted us to analyze focal adhesion dynamics. We found that the rates of focal adhesion assembly and disassembly were faster in Shot-depleted cells, leading to faster adhesion turnover that could underlie the increased migration speeds. This regulation of focal adhesion dynamics may be dependent on Shot being in an open confirmation. Using *Drosophila* border cells as an in vivo model for cell migration, we found that RNAi depletion led to precocious border cell migration. Collectively, these results suggest that spectraplakins not only function to cross-link the cytoskeleton but may regulate cell–matrix adhesion.

INTRODUCTION

Cell migration requires dramatic and continual rearrangements of the two major cytoskeletal systems: actin and microtubules. Historically, microtubules have been viewed as the cell's compass, polarizing toward the direction of migration while simultaneously probing the cytoplasm as a function of dynamic instability (Mitchison and Kirschner, 1984; Gundersen and Bulinski, 1988; Waterman-Storer

and Salmon, 1997). These dynamics in turn communicate to the actin cytoskeleton, or the cell's protrusion machinery. Microtubule polymerization is linked to the activation of the small GTPase Rac and Arp2/3-dependent actin branching, while microtubule depolymerization results in the activation of cellular contractility through the small GTPase Rho and nonmuscle myosin II (Gundersen and Bulinski, 1988; Waterman-Storer *et al.*, 1999; Rooney *et al.*, 2010; Dogterom and Koenderink, 2019; Seetharaman and Etienne-Mann-eville, 2020). Molecules poised to interface with both the actin and microtubule cytoskeletons are therefore critical to our fundamental understanding of cell migration.

The spectraplakin family of proteins are well positioned to mediate coordination between actin and microtubules (Röper *et al.*, 2002; Jefferson *et al.*, 2004; Dogterom and Koenderink, 2019). Spectraplakins are hypothesized to be rod-shaped bivalent molecules that bind actin through N-terminal calponin homology (CH) domains and microtubules through both a lattice-binding growth-arrest–related (GAR) domain and several Sx(I/L)P motifs that target proteins to the plus end of growing microtubules through an association with end-binding proteins (EBs) (Slep *et al.*, 2005; Honnappa *et al.*, 2009; Applewhite *et al.*, 2010; Suozzi *et al.*, 2012;

Hahn et al., 2016; Voelzmann et al., 2017). The N- and C-termini of spectraplakins are separated by an extended rod composed of plakin domains and plectin and spectrin repeats that are predicted to be flexible (Grum et al., 1999; Mirijanian et al., 2007). Spectraplakins can also bind intermediate filaments via plectin repeats, this being particularly relevant to mammalian and *Caenorhabditis elegans* family members as cytoplasmic intermediate filaments appear to be absent in *Drosophila* (Adams et al., 2000; Choi et al., 2002; Jefferson et al., 2004; Guo et al., 1995. Flies do express an atypical tropomyosin isoform (Tm1-I/C) that has been hypothesized to function as an intermediate filament; however, it has yet to be explored whether Short stop (Shot) interacts with Tm1-I/C (Cho et al., 2016). Another commonality among this family of proteins is the large number of alternative splice variants that are present in all of the model organisms of which spectraplakins have been studied (Bernier et al., 1996; Jefferson et al., 2006; Gally et al., 2016; Hu et al., 2016). These splice variants generate even more diversity to this already modular protein family, resulting in isoforms with differing N-terminal leader sequences, single CH domains, changes to the length of central rod domain, and variations to the plakin or plectin domains. Expression of these various isoforms is tissue specific as well, and thus the coordination of actin–microtubule cross-linking by spectraplakins can differ between cell types (Röper and Brown, 2003; Jefferson et al., 2006; Goryunov and Liem, 2016).

The role of spectraplakins in cell migration has been thoroughly studied in mice, where there are two family members, ACF7 and BPAG1. Owing to embryonic lethality, studies of ACF7 in mice have been limited to the analysis of tissues or cells derived from knockout mouse ACF7-deficient endodermal which cells were found to migrate slower and are unable to maintain polarity as assessed by scratch-wound assay (Kodama et al., 2003). Similarly, wounds in the epidermis of ACF7-deficient mice also showed a delay in healing both in vivo through mouse skin grafts and in tissue culture systems (Wu et al., 2011). In these cells, microtubules were uncoupled from the actin cytoskeleton specifically at stress fibers that terminate at focal adhesions. This lack of coordination between actin and microtubules led to defects in the rates of assembly and disassembly of focal adhesions, resulting in larger, less dynamic structures and a subsequent slowing of cell migration. Interestingly, when analyzed in culture, the slower rates of migration could be reverted to wild-types rates by decreasing the concentration of the extracellular matrix on which the cells were plated. Unlike ACF7 knockout mice, BPAG1 mutant mice do survive to adulthood but display sensory defects and muscle degeneration (Guo et al., 1995). However, keratinocytes derived from patients with homozygous nonsense mutations in BPAG1e, an isoform of BPAG1 implicated in epidermolysis bullosa, exhibited increased rates of cell migration and directionality. They were larger in size compared with their wild-type counterparts and had reduced β4 integrin surface levels while also having increased keratin-14 and β1 integrin expression levels (Michael et al., 2014). The increase in β integrin expression corresponded to an increase in surface expression levels as well. These results suggest that the loss of BPAG1e leads to a switch in adhesion types, shifting from a hemidesmosomal-dependent mode to one that depends on integrins and focal adhesions (Michael et al., 2014).

Given the apparent contradiction between data generated in kerotinocyte-deficient BPAG1 and in cells and tissues derived from ACF7 knockouts, we wanted to test the role of spectraplakin-mediated actin–microtubule cross-linking during cell migration in a system with less potential for redundancy. The *Drosophila* genome, which contains a single spectraplakin family member, Short stop (Shot), gives us this opportunity. We used both cell-based assays as well as an in vivo assay for cell motility to understand the role of Shot during cell migration. While more closely related to ACF7 than BPAG1, our results indicate that the RNA interference (RNAi) depletion of Shot leads to an increase in cell migration, similar to what has been described of keratinocytes derived from *dst* patients. Furthermore, the well-established connection between cell–matrix adhesion and migration speed as well as the previous literature regarding the effects of ACF7 and BPAG1 knockout on focal adhesion dynamics led us to further examine focal adhesion turnover in Shot-depleted cells. Quantification of focal adhesion assembly and disassembly rates revealed that, contrary to the more stable focal adhesions observed following ACF7 depletion, Shot-depleted cells exhibited significantly higher rates of both assembly and disassembly compared with control-treated cells, resulting in faster focal adhesion turnover. Our results also indicate that its role in focal adhesion dynamics is dependent on Shot's ability to cross-link actin and microtubules.

RESULTS

To interrogate Shot's role in cell migration in a system with less potential for redundancy, we choose three motile *Drosophila* tissue culture cells lines, ML-DmD17c3 (D17) derived from third instar larval haltere discs, ML-DmD25c2 (D25) derived from third instar wing discs, and Ras^{V12};wts^{RNAi} (Ras^{V12}) cells, which are immortalized epithelial-like cell–derived homogenized fly embryos expressing the UAS- RasV12 oncogene, a hairpin RNAi construct for warts (wts), a tumor suppressor gene, and GFP, driven by the actin5C-Gal4 promoter (Ui et al., 1987; Simcox et al., 2008). These cell lines are readily available through the Drosophila Genomics Resource Center (DGRC. When plated on a mixture of extracellular matrix (ECM) proteins that we harvest and concentrate from the cell culture media of confluent D25 cells (Rogers and Rogers, 2008; Currie and Rogers, 2011), these cells polarize and form cell–matrix adhesions similar to mammalian tissue culture cells forming multiprotein, plaque-like structures distributed at a cell's periphery. These focal adhesions contain classic ECM receptors, integrins (Figure 1, A–C), and other well-characterized focal adhesion proteins such as Vinculin and p130CAS. Furthermore, Ras^{V12} cells maintain these cell–cell junctions as they migrate (Figure 1D). Similar to other *Drosophila* tissues, these cells are acentrosomal during interphase and thus represent an opportunity to study the interactions between actin and microtubules in the absence of a functional centrosome (Figure 2, A and B; Supplemental Movie S1) (Rogers et al., 2008; Currie and Rogers, 2011). Previously, we characterized the Shot A isoform (ShotA-EGFP) in *Drosophila* S2 cells and found that Shot localized both to the plus ends of microtubules as well as along the length of the microtubules found in the periphery of these cells (Applewhite et al., 2010). When we expressed this same construct in D17 and D25 cells, we observed a similar microtubule localization (Figure 2C) as well as localization to a subset of focal adhesions, colocalizing with mCherry-Vinculin (Figure 2D). This finding is in line with previous reports that found Shot localizing to sites of cell–matrix and cell–cell adhesion such as myotendinous junctions or between follicular epithelia in vivo (Gregory and Brown, 1998; Subramanian et al., 2003). Furthermore, this localization is similar to what has been reported for the mammalian spectraplakin ACF7, which colocalizes with focal adhesions (Wu et al., 2011; Yue et al., 2016).

Depletion of Shot leads to an increase in cell migration speeds

We treated both D17 and D25 cells with Shot and control RNAi as well as RNAi that targets the Rho family GTPases Rac1, Rac2, and
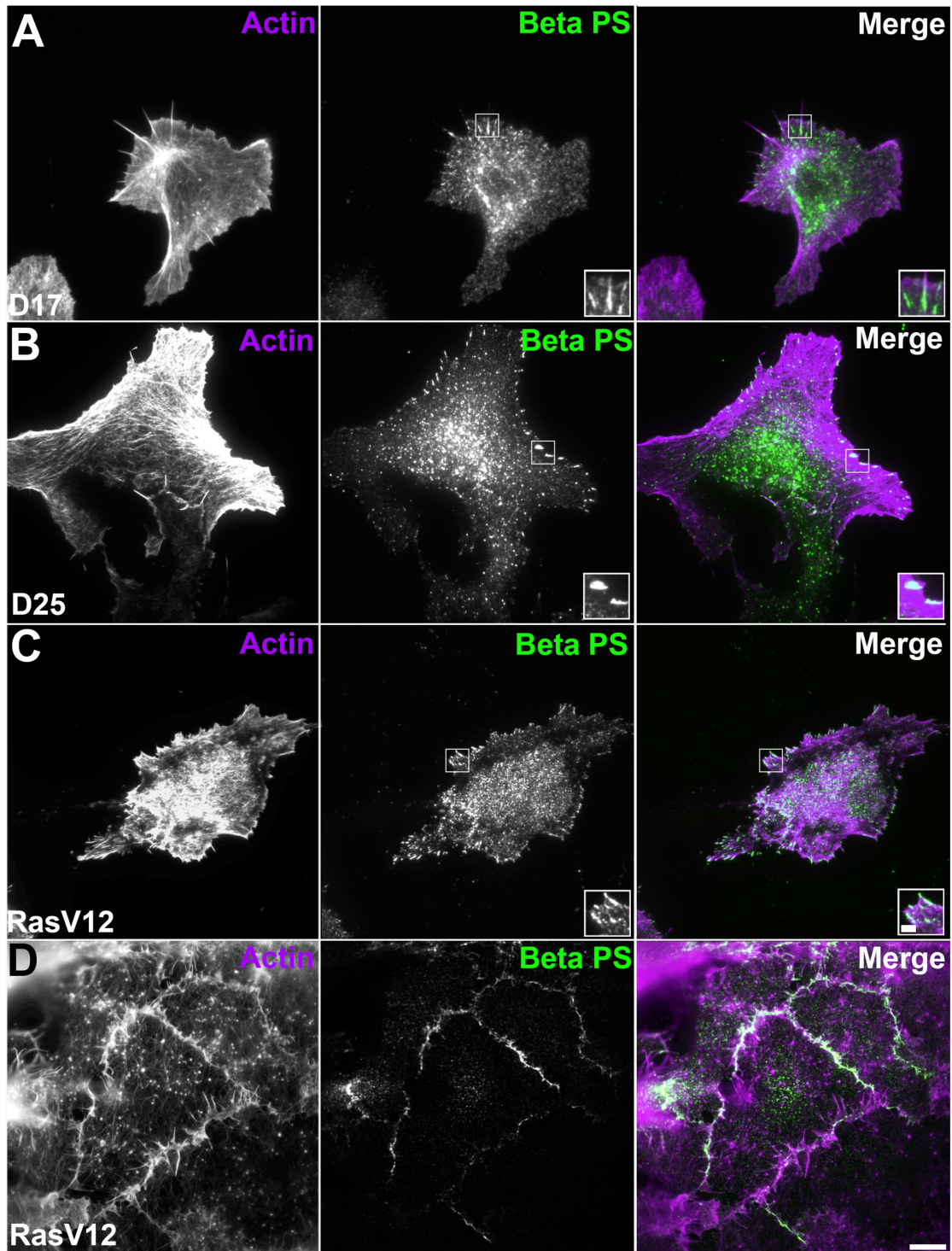
FIGURE 1: Migratory *Drosophila* cells form cell–matrix and cell–cell adhesions in a manner similar to that of mammalian tissue culture cells. (A–D) Migratory *Drosophila* epithelial cells plated on ECM imaged by TIRF microscopy. (A) *Drosophila* D17 fixed and immunostained for phalloidin to mark F-actin (purple in merged image) and βPS integrin (green in merged image). The white box denotes βPS integrin staining indicative of cell–matrix adhesions and is shown at higher magnification. (B) *Drosophila* D25 cell fixed and immunostained for phalloidin to mark F-actin (purple in merged image) and βPS integrin (green in merged image) to mark cell–matrix adhesions. The white box denotes βPS integrin staining indicative of cell–matrix adhesions and is shown at higher magnification. (C) *Drosophila* Ras^V12 cells fixed and immunostained for phalloidin to mark F-actin (purple in merged image) and βPS integrin (green in merged image) to mark cell–matrix adhesions. The white box denotes βPS integrin staining indicative of cell–matrix adhesions and is shown at higher magnification. (D) *Drosophila* Ras^V12 plated at cell density to allow for the formation of a sheet, fixed and immunostained with phalloidin to mark F-actin (purple in merged image) and βPS integrin (green in merged image). Note that βPS integrin both localizes to discrete puncta (C) as well as at sites of cell–cell adhesions. Scale bar 10 μm in low-magnification images and 2 μm in high-magnification images.
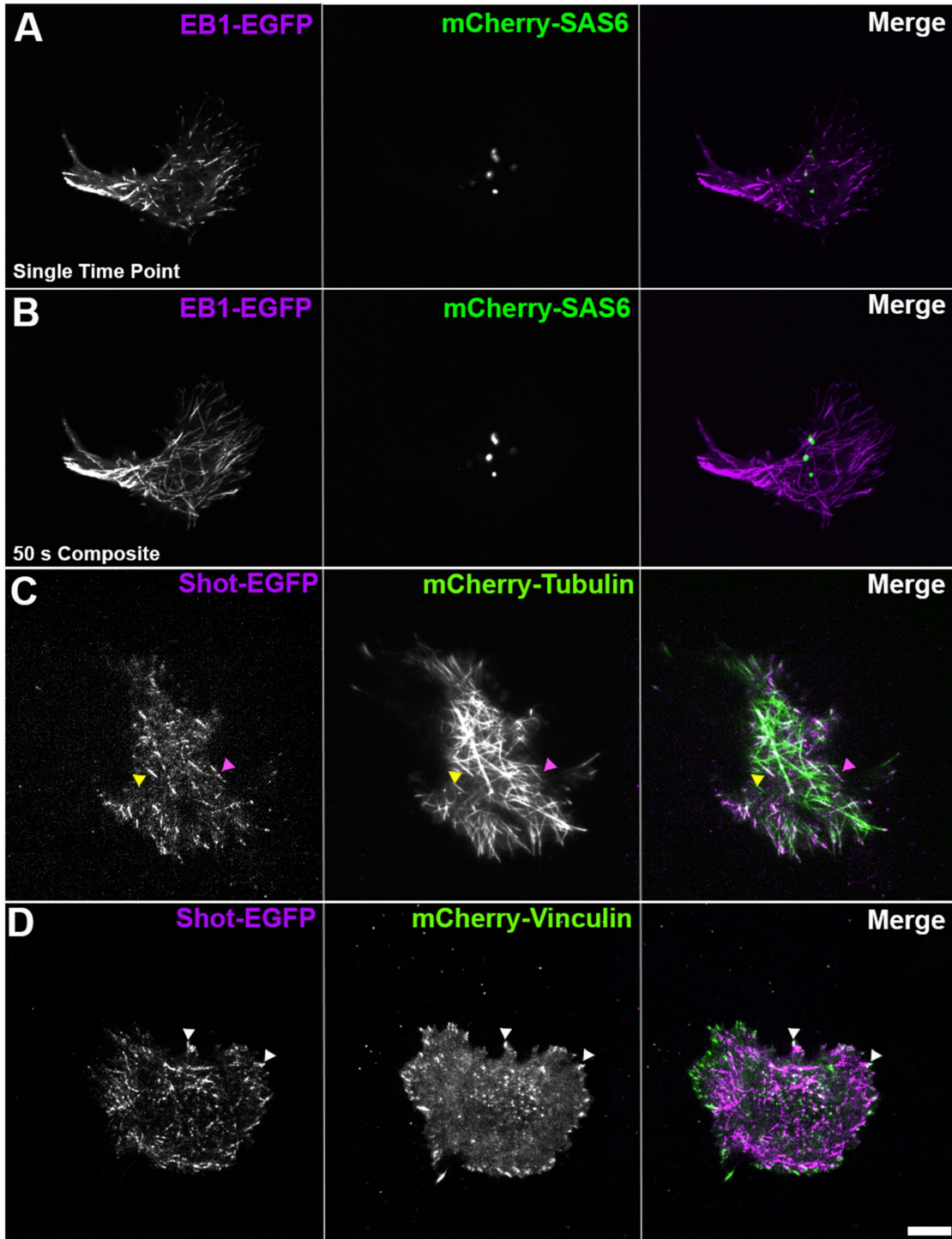
FIGURE 2: Shot localizes to the lattice and plus ends of microtubules, which are arranged in an acentrosomal microtubule array during interphase. (A–D) *Drosophila* D25 cells imaged by TIRF microscopy. (A) D25 cell coexpressing EGFP-tagged EB1 (purple in merged image) and mCherry-SAS6 (green in merged image), a marker of centrioles. (B) A 50 s composite image of the cell shown in A; note that the EB1 comets are not originating from the SAS6 marked centrioles. (C) D25 cell coexpressing Shot A-EGFP (purple in merged image) and mCherry-tagged tubulin (green in merged image). The yellow triangle indicates Shot's association with the plus end of a microtubule, while the magenta triangle indicates a region of the cell where Shot is associated with the lattice of the microtubule. (D) D25 cell coexpressing Shot A tagged with EGFP (purple in merged image) and mCherry-tagged Vinculin (green in merged image). White triangles denote the colocalization of Shot with the focal adhesion marker Vinculin. Scale bar 10 µm.

Mig-2-like (Rac/Mtl), which served as positive control cells given their established role in cell migration (Raftopoulou and Hall, 2004; Lawson and Burridge, 2014; Mayor and Etienne-Manneville, 2016).

Throughout the article Shot RNAi refers to a double-stranded RNA (dsRNA) template designed against Shot's 3'-untranslated region (3'UTR) first characterized in Applewhite *et al.* (2010). This 3'UTR
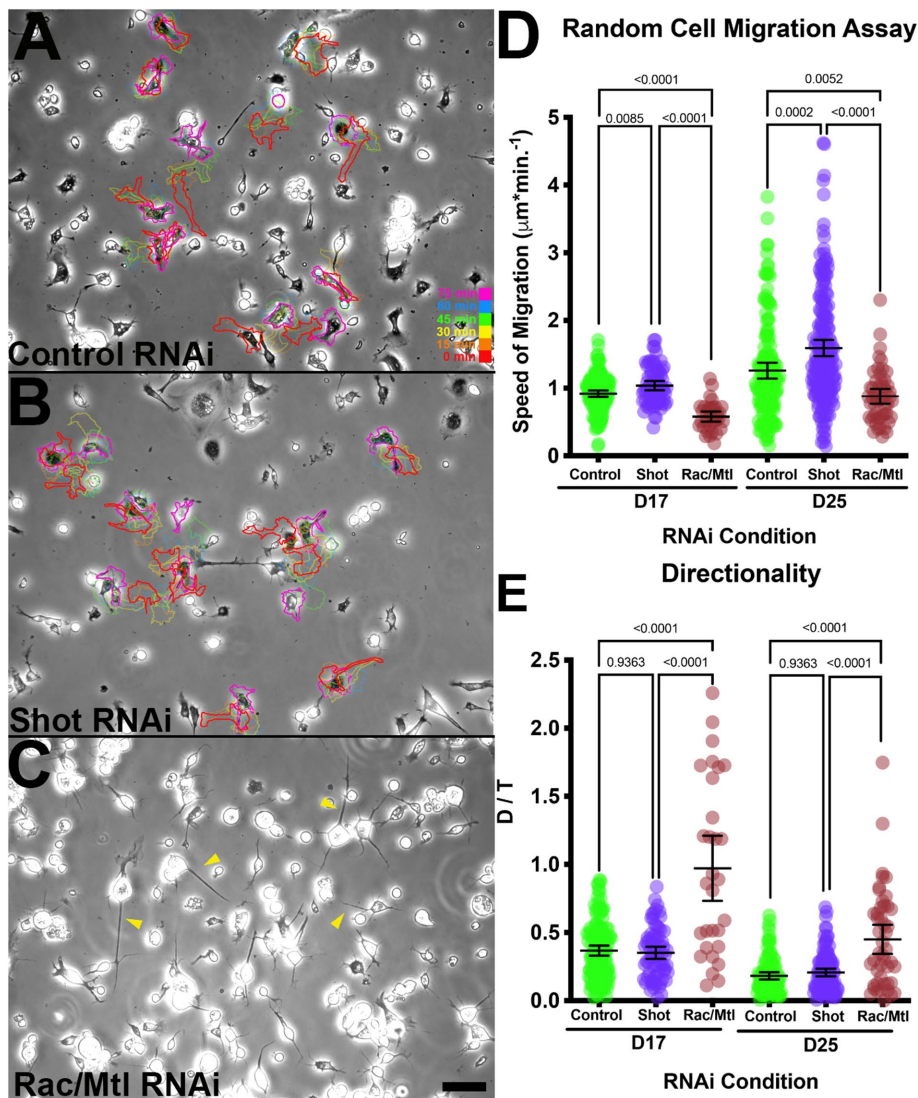
FIGURE 3: RNAi depletion of Shot increases cell migration speeds. Phase-contrast images of *Drosophila* D25 cells following treatment with (A) control RNAi, (B) Shot RNAi, or (C) Rac/Mtl RNAi. Scale bar 20 μm. Cell positions in Shot- and control RNAi-treated cells are marked by outlines at time 0 min (red), 15 min (orange), 30 min (yellow), 45 min (green), 60 min (blue), and 75 min (purple). (C) Rac/Mtl cells failed to substantially migrate so this denotation was omitted; yellow triangles mark processes the result of RNAi treatment. (D) Scatter plot of cell migration speeds with control RNAi-treated cells (green), Shot RNAi–treated cells (purple), and Rac/Mtl (maroon). D17 cells (*p* value < 0.0001, *N* = 3, 136 control cells, 70 Shot-depleted, and 33 Rac/Mtl-depleted cells) and D25 cells (*p* value < 0.0001, one-way analysis of variance [ANOVA], *N* = 3, 149 control RNAi-treated cells, 190 Shot-depleted cells, and 52 Rac/Mtl-depleted cells) exhibit a statistically significant increase in cell migration speeds following Shot depletion and a statistically significant decrease in cell migration speeds following Rac/Mtl RNAi. (E) Scatter plot of cell directionality (D/T) of control RNAi-treated (green circles), Shot-depleted (purple circles), and Rac/Mtl-depleted (maroon circles) cells for both D17 (130 control RNAi-treated cells, 70 Shot- depleted cells, and 30 Rac/Mtl-depleted cells) and D25 (100 control treated cells, 111 Shot-depleted cells, and 53 Rac/Mtl-depleted cells). Cell directionality was calculated as a ratio of the direct distance between start and end points (D) to the total path length taken by the cells (T). There was no statistically significant difference in directionality between Shot and control RNAi-treated cells, while there was a statistically significant increase in directionality for Rac/Mtl RNAi-treated cells (*p* value < 0.0001, one-way ANOVA).

Shot dsRNA region is shared by nearly all Shot isoforms (see *Materials and Methods*). The control RNAi used throughout this article is designed against the pBluescript vector, which lacks sequence homology to the *Drosophila* genome. Following a 7-d

course of RNAi treatment, we plated the cells on *Drosophila*-derived ECM. When plated to subconfluency, these cells migrate randomly and can be imaged by phase-contrast microscopy over extended periods of time. We imaged the RNAi-treated cells for 3–6 h and tracked their migration (Figure 3, A–C). Control RNAi-treated D17 cells migrated at a rate of 0.92 ± 0.02 μm/min SEM; however, we observed a modest but statistically significant increase in the rate of migration following Shot depletion (1.04 ± 0.03 μm/min SEM), while the average migration speed of Rac/Mtl RNAi–treated cells was considerably slower (a statistically significant 0.58 ± 0.04 μm/min SEM) (Figure 3D). Following a similar protocol, we depleted control, Shot, and Rac/Mtl in D25 cells and found that control RNAi-treated D25 cells migrate slightly faster (1.26 ± 0.06 μm/min SEM) than D17 cells and display a more robust increase in cell migration following Shot depletion (1.6 ± 0.06 μm/min SEM) (Figure 3C; Supplemental Movies S2–S4). This was a statistically significant 28% increase in the speed of cell migration. Similar to D17 cells, depletion of Rac/Mtl in D25 cells also led to a statistically significant decrease in migration speeds (0.88 ± 0.05 μm/min SEM). Also apparent in Rac/Mtl-depleted cells was the formation of long projections as opposed to Arp2/3-generated lamellipodia and an increase in the number of phase-light cells indicative of an inhibition of adhesion (Figure 3C) (Machesky *et al.*, 1994; Mullins *et al.*, 1998; Svitkina and Borisy, 1999). We also measured the directionality of both cell types following RNAi treatments and did not observe any statistically significant differences between Shot and control RNAi-treated cells (Figure 3E). Rac/Mtl RNAi–treated cells showed a robust increase in directionality as compared with Shot- and control-treated cells, but this is likely a consequence of the substantial decrease in migration speeds and our method used to calculate directionality (Figure 3E). There are two mammalian spectraplakins, ACF7 and BPAG1/*dst*; the increase in migration speeds that we observed upon Shot depletion is reminiscent of phenotypes reported for keratinocytes derived from *dst* patients rather than for loss of ACF7 (Kodama *et al.*, 2003; Michael *et al.*, 2014; Yue *et al.*, 2016).

Depletion of Shot alters lamellipodial dynamics
To investigate the mechanism behind this increase in cell migration, we tracked the dynamics of the cell periphery. We transfected D25 cells with EGFP-actin, imaged them by total internal reflection
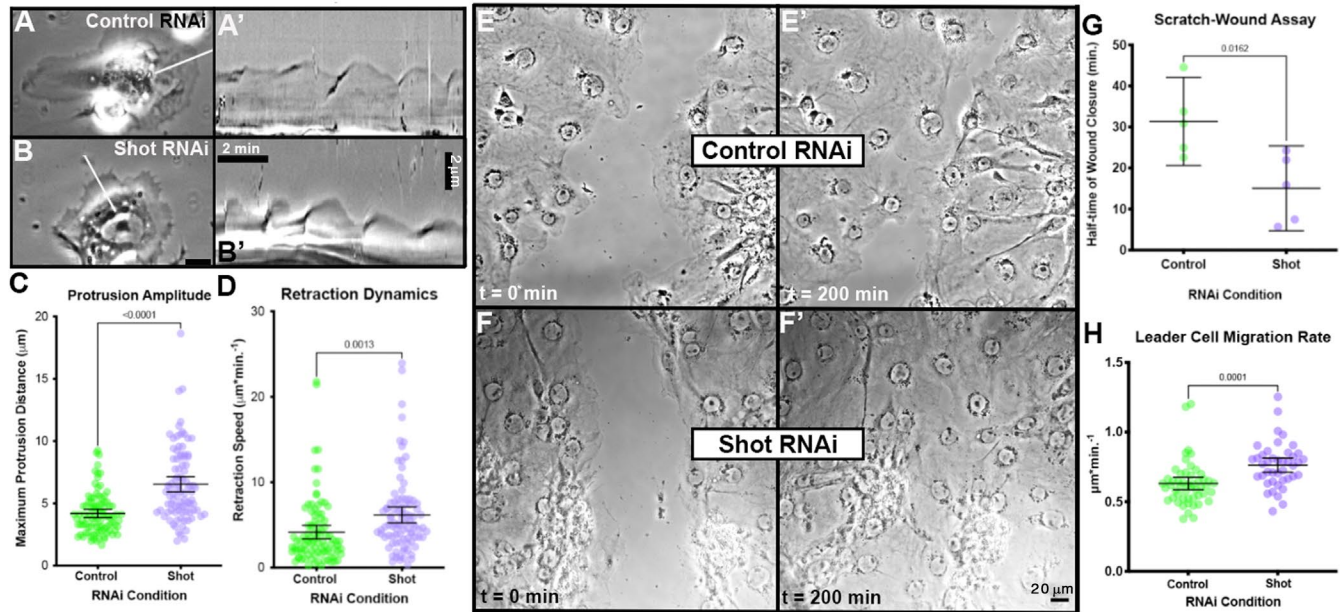
FIGURE 4: Shot depletion increases the amplitude of lamellipodial protrusions and the speed of retraction as well as the rate of collective cell migration. (A, B) *Drosophila* D25 cells were imaged by phase-contrast microscopy following treatment with (A) control or (B) Shot RNAi; then (A′, B′) kymographs were generated to measure lamellipodial dynamics. Scale bars 10 µm in low-magnification images and 2 min and 2 µm in kymographs. (C) Scatter plot of the maximum lamellipodial protrusion distance (µm) as measured from kymographs generated from phase-contrast movies of control (green) and Shot-depleted (purple) cells. There was a statistically significant increase in the maximum protrusion distance (*p* value < 0.0001, Student's *t* test, *N* = 3, 94 control treated cells and 92 Shot RNAi–treated cells). (D) Scatter plot of the lamellipodial retraction speed (µm*min^{-1}) as measured from kymographs generated from phase-contrast movies of control (green) and Shot-depleted (purple) cells. There was a statistically significant increase in the retraction speed in Shot-depleted cells as compared with control RNAi-treated cells (*p* value = 0.0013, Student's *t* test, *N* = 3, 94 control treated cells and 92 Shot RNAi–treated cells). Phase-contrast images of Ras^{V12} cells (E and F) before wound closure and (E′ and F′) following 200 min. Cells were treated with control RNAi (E and E′) or Shot RNAi (F and F′). Scale bar 20 µm. (G) Scatter plot of the half-time of wound closure for control RNAi-treated (green) and Shot RNAi–treated (purple). Half-times were calculated by measuring the rate of area change of the wound over time. There was a statistically significant decrease in the half-time of wound closure in Shot depleted cells as compared with control RNAi-treated cells (*p* value = 0.0162, Student's *t* test, *N* = 5). (H) Scatter plot of leader cell migration rate from the scratch-wound assays. Cells were treated with control RNAi (green circles) or Shot RNAi (purple circles) with each data point representing an average speed for one cell (*N* = 3, *n* = 51 and 42 cells, respectively). There was a statistically significant increase in the leader cell migration rate (*p* value 0.0001, Student's *t* test).

fluorescence (TIRF) microscopy, and then quantified cell shape change over time as a proxy for peripheral dynamics (Supplemental Figure 1). When plated on their own ECM, the peripheral dynamics of D25 cells largely mimic that of mammalian cells with rapid fluctuations between periods protrusion and retraction (Supplemental Figure 1, A and B). Depletion of Shot led to a statistically significant increase in peripheral dynamics as compared with control RNAi-treated cell (*p* = 0.0198, Student's *t* test; Supplemental Figure 1D). This difference was eliminated once these cells were plated on concanavalin A (con A), a lectin, which likely does not engage signaling through cell–matrix adhesions (Supplemental Figure 1, C and D) (Rogers *et al.*, 2003).

While the above analysis captures macro changes to the cell periphery, the lamellipodia undergoes specific phases of protrusion and retraction, which contributes to the overall rate of cell migration (Cramer, 1999; Small *et al.*, 2002; Small and Resch, 2005; Ponti, 2004). We used phase-contrast microscopy in combination with kymography to capture these parameters (Hinz *et al.*, 1999; Bear *et al.*, 2002; O'Connell *et al.*, 2019). Specifically, we were able to measure the frequency, persistence, and amplitude of these protrusions, as well as the speed of lamellipodial retraction (Figure 4, A, A′, B, and B′). While there were no statistically significant differences in the

speed, persistence, or frequency of protrusions between control and Shot RNAi–treated cells (Supplemental Figure 2, A–C), we did observe a statistically significant increase in the amplitude of these protrusions (*p* value < 0.001, Student's *t* test) and the rate of retraction (*p* value = 0.0013, Student's *t* test). During lamellipodial protrusion, adhesion through integrins stabilizes the lamellipodia, effectively anchoring it in place (Galbraith *et al.*, 2007; Petrie *et al.*, 2009). The increase in lamellipodial dynamics that we observe following Shot depletion, specifically the increase in the amplitude of the protrusions and the speed of retraction, may be indicative of weaker adhesion throughout the lamellipodia and less anchoring through integrins.

Depletion of Shot also increases the rate of collective cell migration

Ras^{V12} cells are invasive and exhibit metastatic migration when injected into the abdomen of adult flies (Simcox *et al.*, 2008). Because these cells maintain cell–cell adhesion as they migrate, they are ideal for performing a scratch-wound assay (Figure 4, E–H). Following a similar 7 d course of RNAi, we depleted cells of Shot or treated them with control RNAi. Similar to what we observed in the D17 and D25 cells, Shot-depleted Ras^{V12} cells migrated faster than control
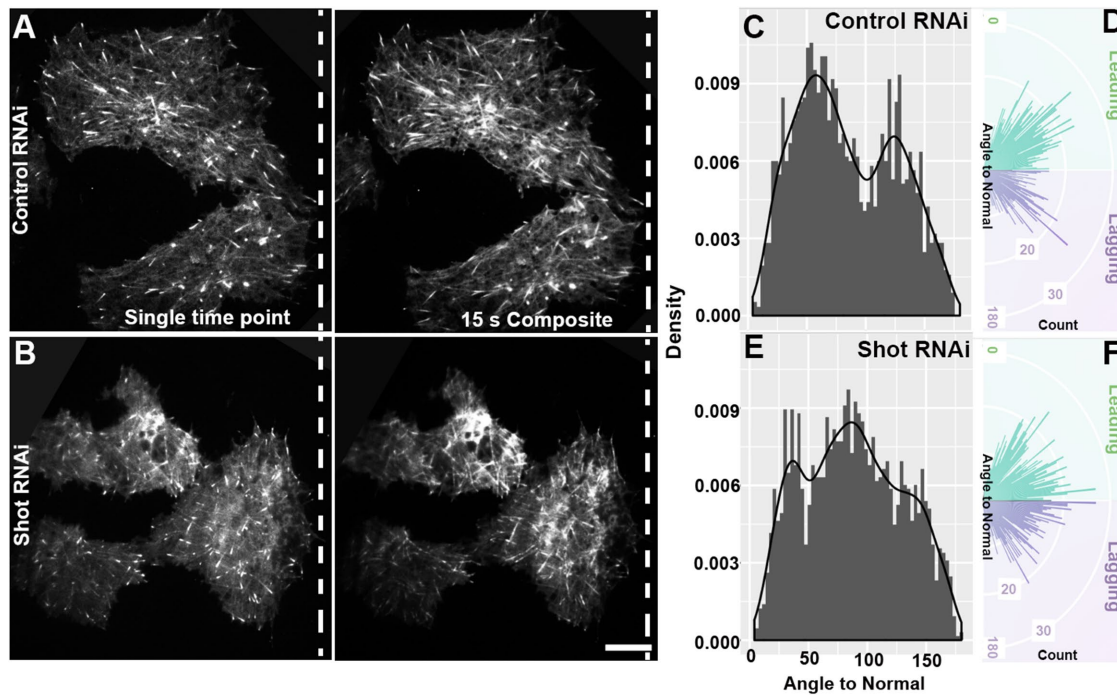
FIGURE 5: Shot depletion disrupts microtubule polarity of directionally migrating cells. (A, B) Ras^{V12} imaged by TIRF following treatment with (A) control RNAi or (B) Shot RNAi. Cells were plated to form a monolayer and a scratch-wound assay was performed following transfection with TagRFP-EB1. As cells migrated to close the wound, the angle of microtubule polymerization was measured via EB1 comet trajectories. The wound edge is denoted by the dotted lines. EB1 comets polarized toward the wound edge are false-colored green while those not polarized toward the wound edge are false-colored pink. Scale bar 10 μm. (C, D) Histograms reflect the counts of the angle of EB1 comet trajectories relative to the normal of the wound. A density plot is superimposed to better visualize the distribution of the data. (C) Control RNAi-treated cells exhibited in a bimodal distribution of EB1 comet trajectories indicating microtubule polarity toward and away from the wound while (D) Shot RNAi–treated cells resulted in a gaussian distribution reflecting the mixed polarity of EB1 comet trajectories. (E, F) Circular histograms that reflect the counts of the angles of EB1 trajectories with respect to the normal for cells treated with (E) control RNAi and (F) Shot RNAi. EB1 comet angles were binned from zero to 180 with those polarized toward the leading edge shaded in green while those polarized toward the trailing edges of the cell are shaded in purple. Note a biomodal distribution of the EB1 angles in the control treatment, whereas Shot depletion led to a more equal distribution of angles, indicating a loss of microtubule polarity.

treated cells, resulting in a statistically significant shorter half-time of wound closure (p value = 0.0162, Student's t test) (Figure 4G). We also measured the rate of leader cell migration and again found that Shot depletion led to a statistically significant increase in migration speeds (p value = 0.0001, Student's t test) (Figure 4H). We note that this trend is the inverse of the delayed wound closure times observed in ACF7 knockdown mammalian cells (Wu *et al.*, 2008; Yue *et al.*, 2016). Thus, depletion of Shot appears to increase the rate of both random cell migration and collective cell migration in *Drosophila* tissue culture cells.

Shot depletion disrupts microtubule polarity during directed cell migration

During cell migration, microtubules have been observed polarizing in the direction of migration, where it has been shown that microtubule polymerization signals to the actin cytoskeleton through the Rho family of GTPases. Subsequent activation of the small GTPase Rac at the leading edge leads to Arp2/3-mediated actin branching and lamellipodia formation (Waterman-Storer and Salmon, 1997; Waterman-Storer *et al.*, 1999). Knockout or depletion of ACF7 in different mammalian cell lines resulted in a disorganized microtubule array including a loss in this leading edge microtubule polarity, a factor that may also influence the migration of ACF7-deficient cells (Kodama *et al.*, 2003; Wu *et al.*, 2011). Given the contradictory

cell migration results that we observed in *Drosophila* tissue culture cells, we wondered whether Shot also functions to maintain microtubule polarity in fly cells. To induce directed cell migration, we used a scratch-wound assay. During a scratch-wound assay, cells reorient, polarizing in the direction of the "wound." We can therefore predict the direction of cell migration following the wounding of the monolayer and thus the orientation of the microtubule network. Ras^{V12} cells were treated with a 7-d course of RNAi targeting Shot or control and were then transfected with EB1 tagged with RFP to mark the growing plus ends of microtubules (Figure 5, A and B). The cells were then plated at a density that allowed for the formation of epithelial-like sheets. A wound was etched into each sheet, leading to the polarization and migration of the cells to close the wound. During polarization and migration, we imaged the growing microtubule plus end using live-cell TIRF microscopy and measured the angle between the direction of migration and the trajectory of EB1 comets (Figure 5, C–F). The distribution of angles for control RNAi cells (n = 1890 microtubules) was bimodal with two maxima around 58 and 129°, indicating a leading–lagging edge polarity as the majority of microtubule polymerization was aligned in the direction of migration (Figure 5, C and D). However, following Shot depletion the microtubule polymerization angles had a normal distribution with a single peak roughly at 87° (n = 2160 microtubules; Figure 5, E and F). This indicates that rather than being polarized in the direction of

migration, the orientation of microtubule polymerization was random. These results indicate that, similar to ACF7 in mammalian cells, Shot maintains microtubule polarity in fly cells as they migrate. However, despite this loss of microtubule polarity in the direction of migration, Shot-depleted cells continue to migrate faster.

Shot depletion increases the rate of focal adhesion disassembly

The faster rate of migration displayed by Shot-depleted cells prompted us to examine focal adhesion dynamics. Cell–matrix adhesion is regulated through rates of focal adhesion turnover (Delorme-Walker et al., 2011) and impacts the closely related processes of force generation and migration speeds (Burridge and Chrzanowska-Wodnicka, 1996; Beningo et al., 2001; Schratt et al., 2002; Gupton and Waterman-Storer, 2006; Gupton et al., 2007). To measure rates of adhesion turnover, we treated D25 cells with Shot or control RNAi and then transfected them with mCherry-Vinculin (Figure 6, A and B), an established marker of focal adhesions (Ribeiro et al., 2014; Ivanova et al., 2017). Using TIRF microscopy, we recorded movies of focal adhesion assembly and disassembly and then fitted the fluorescence intensity measurements over time in order to derive the rate constants for the two processes (Stehbens et al., 2014). Rate constants for assembling focal adhesions were drawn from focal adhesions found at the leading edge of migrating D25 cells, while rate constants for disassembly were drawn from focal adhesions found at both the leading and trailing edge of the cells. This analysis revealed that both focal adhesion assembly and disassembly rate constants were significantly higher in Shot-depleted cells ($p = 0.0035$ and < 0.0001, respectively, Student's t test) as compared with control RNAi-treated cells, indicative of faster focal adhesion assembly and disassembly and shorter overall focal adhesion lifetimes (Figure 6, C and D). Despite these differences in focal adhesion assembly and disassembly rates, we did not observe any major differences in focal adhesion distributions between control and Shot-depleted cells (Supplemental Figure 3, A and B). Further, when we compared focal adhesion areas between control and Shot-depleted cells, there was not a statistically significant difference (Supplemental Figure 3E). This correlation between faster migration and increased disassembly and assembly rates is consistent with the observations of previous studies investigating other regulators of focal adhesion dynamics, where the phenotype of faster migration correlated with faster focal adhesion turnover (Nayal et al., 2006; Hu et al., 2017; Wang et al., 2018). The greater rate of focal adhesion turnover in Shot-depleted cells is the opposite of the more stable, longer-lived focal adhesions observed in mammalian cells upon depletion or loss of ACF7 (Wu et al., 2008; Yue et al., 2016). This contrast in focal adhesion dynamics may contribute to the differential speeds of cell migration between mammalian and fly cells following spectraplakin depletion as rapid adhesion turnover or the efficient disassembly of old adhesions and the formation of new ones is crucial for protrusion and migration (Laukaitis et al., 2001; Webb et al., 2004; Hu et al., 2015).

Shot's intramolecular conformation plays a role in its colocalization with focal adhesions

The altered focal adhesion dynamics that resulted from Shot depletion led us to examine the relationship between Shot and focal adhesion proteins more closely. In *Drosophila* tendon cells, Shot colocalizes with βPS integrin and paxillin, key components of focal adhesions (Subramanian et al., 2003). Furthermore, Shot is also highly expressed in the epidermis of developing *Drosophila* embryos at the same sites of integrin-mediated adhesion, and deple-

tion or loss of Shot in wing discs phenocopies the loss of cell–matrix adhesion proteins, leading to wing blistering (Prout et al., 1997; Gregory and Brown, 1998). To further explore this relationship, we coexpressed EGFP-tagged Shot with mCherry-Vinculin in D25 cells and then quantified the degree of colocalization using Mander's overlap coefficient (MOC) (Figure 7). MOC expresses the degree to which two structures spatially overlap, taking into account the total amount or abundance of fluorophores that overlap to produce a value that ranges from zero (no overlap) to one (perfect colocalization) (Dunn et al., 2011). It is important to note that only a subset of Vinculin-containing focal adhesions also contained Shot; however, a similar trend can be observed with Shot's mammalian counterpart ACF7 in mammalian focal adhesions (Wu et al., 2008). We compared the MOC for Shot and Vinculin to that of Vinculin and p130CAS, which is predicted to have a high MOC for both values (that amount of Vinculin overlapping with p130CAS and the amount of p130CAS overlapping with Vinculin) as well as an untagged GFP as a negative control (Figure 7, A–C, F, and G). As expected, there was a large degree of colocalization between p130CAS and Vinculin, whereas the degree of colocalization between Shot and Vinculin was lower, a reflection of the subset of focal adhesions that contain Shot (Figure 7, A, C, and F). In summary, Shot is found at many but not all focal adhesions, a localization pattern consistent with what has been observed in the epidermis of *Drosophila* embryos and in tendon cells (Gregory and Brown, 1998; Subramanian et al., 2003). This is the first demonstration of Shot's localization at focal adhesions in tissue culture cells and may indicate a role for Shot in regulating cell–matrix adhesion dynamics.

Results from our previous work suggested that Shot exists in two conformations, a "closed" conformation where it localizes to the plus tips of microtubules through EB1 but is unable to cross-link actin and microtubules and an "open" conformation where it exhibits both microtubule lattice binding and plus-end tracking and is capable of actin–microtubule cross-linking (Applewhite et al., 2013). To determine whether Shot's localization to focal adhesions is dependent on these conformations, we turned to a previously characterized Shot construct, FKBP-Shot-FRB-EGFP, which is full-length Shot flanked by the tripartite, rapamycin-induced, FKBP/FRB dimerization system (Applewhite et al., 2013). We first treated cells with RNAi targeting the Shot, which primarily targets the endogenous pool of Shot (see *Materials and* Methods), and then transiently expressed FKBP-Shot-FRB-EGFP under the control of metallothionein copper inducible promoter (pMT). The dynamics of FKBP-Shot-FRB-EGFP are indistinguishable from that of Shot A-GFP; however, in the presence of rapamycin this construct is locked in the closed conformation. Using MOC we compared the degree of colocalization between FKBP-Shot-FRB-EGFP and Vinculin with and without the addition of rapamycin (Figure 7, D and E). Upon rapamycin treatment, we observed a decrease in the MOC values that represent Shot's overlap with Vinculin (p value $= 0.0101$, Student's t test) (Figure 7H). There was a similar decrease in the MOC when we quantified the fraction of Vinculin overlapping with Shot; however, this difference was not statistically significant (Figure 7I). While both values display a decrease upon Shot's adoption of the "closed-form" conformation, the discrepancy in the statistical significance of the two decreases in MOC values may be due to the large amount of Vinculin that does not overlap with Shot. These results indicate that Shot's conformation impacts its colocalization with focal adhesions; specifically, the "open" conformation of Shot displays a greater degree of colocalization than Shot in the "closed," cross-linking–inhibited conformation. Further, these findings reveal that, similar to its mammalian homologue ACF7 (Yue et al., 2016), Shot localizes to focal
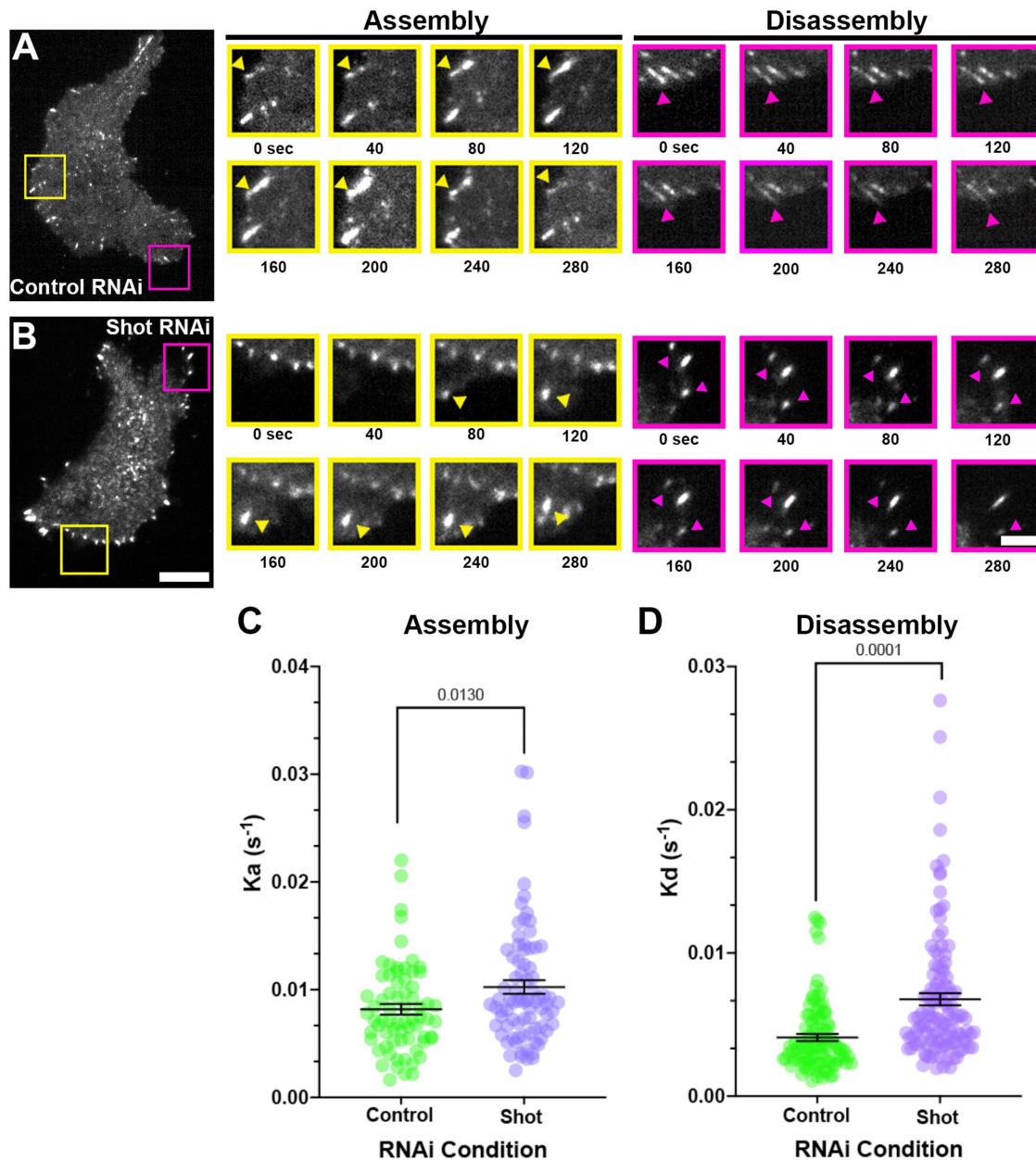
FIGURE 6: Depletion of Shot increases both focal adhesion assembly and disassembly. (A, B) *Drosophila* D25 cells were transfected with mCherry-tagged Vinculin and imaged by TIRF microscopy following treatment with (A) control or (B) Shot RNAi. The yellow boxes in the low-magnification images (scale bar 10 μm) denote regions where focal adhesions were assembling and are shown to the right as a time series (time in seconds) at higher magnification (scale bar 2 μm) with yellow borders. Yellow triangles indicate individual assembling focal adhesions. The magenta boxes in the low-magnification images denote regions where focal adhesions are disassembling and are shown to the right as a time series at higher magnification with magenta borders. Magenta triangles indicate individual disassembling focal adhesions. (C) Scatter plot of the association rate constant (K_a) of focal adhesion assembly for control (green) and Shot-depleted (purple) cells. There was a statistically significant increase in the rate of focal adhesion assembly in Shot-depleted cells (p value = 0.0130, Student's t test, $N = 3$, 61–68 individual focal adhesions from 3–4 cells per condition) as compared with control RNAi treatments. (D) Scatter plot of the dissociation rate constant (K_d) of focal adhesion disassembly for control RNAi (green)- and Shot RNAi (purple)–treated cells. There was a statistically significant increase in focal adhesion disassembly following Shot depletion (p value = 0.0001, Student's t test, $N = 3$, 98–101 individual focal adhesions from 3–4 cells per condition).

adhesions at the resolution of individual cells and discrete adhesions, which has not been previously reported. This corresponding change in localization is not unlike what we observed in Applewhite *et al.* (2013), where cells transfected with FKBP-Shot-FRBEGFP, following perfusion with rapamycin, showed a drastic reduction in Shot's lattice binding behavior as well as an inhibition of actin–microtubule cross-linking as evidenced by the increase in microtubule fishtailing (Applewhite *et al.*, 2013). Thus, Shot's confirmation not only regulates how it interacts with microtubules, but also how it interacts with focal adhesions.
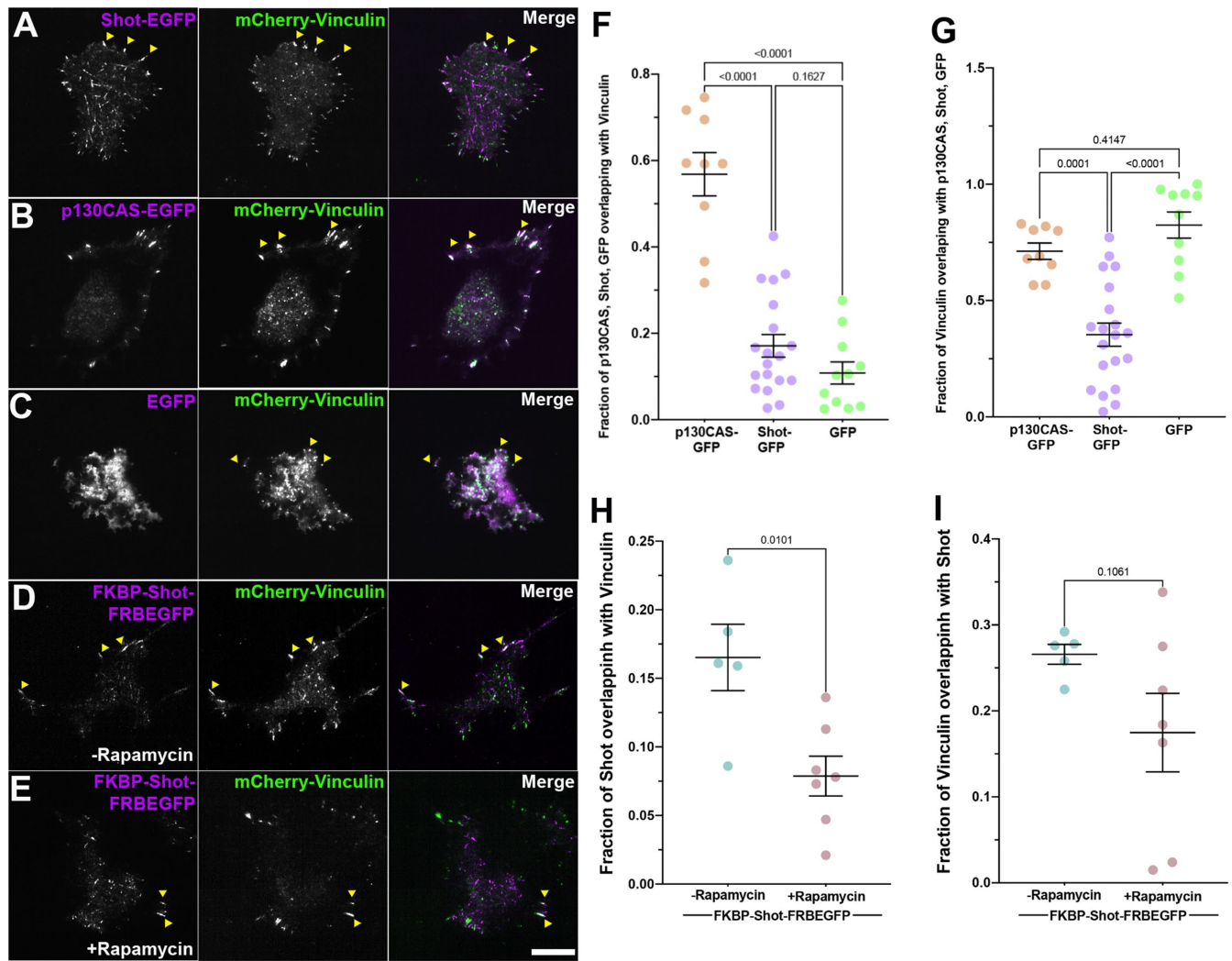
FIGURE 7: Shot's intramolecular conformation regulates its localization to focal adhesions. (A–E) *Drosophila* D25 cells cotransfected with Vinculin (green in merge) and (A) Shot-EGFP, (B) p130CAS-EGFP, (C) untagged-EGFP, (D) FKBP-Shot-FRBEGFP without rapamycin, and (E) FKBP-Shot-FRBEGFP with the addition of 500 nM rapamycin (purple in merge). Yellow arrowheads indicate colocalization between GFP-tagged protein and mCherry-Vinculin. (F, G) Scatter plot of the MOC representing (F) the fraction of p130CAS-EGFP (positive control, orange), Shot-EGFP (purple), and untagged-EGFP (green) overlapping with mCherry-Vinculin. There was a statistically significant difference in the fraction of overlap between p130CAS-EGFP and mCherry-Vinculin (*p* value < 0.0001, one-way ANOVA, *n* = 10–20 cells). (G) MOC for the fraction of mCherry-Vinculin overlapping with p130CAS-EGFP (orange), Shot-EGFP (purple), and untagged-EGFP (green). There was a statistically significant difference in the fraction of Vinculin overlapping with Shot-EGFP and p130CAS-EGFP and untagged-GFP, respectively (*p* value < 0.0001, one-way ANOVA, *n* = 10–20 cells). (H, I) Scatter plot of MOC for cells treated with 3'UTR Shot RNAi and coexpressing mCherry-Vinculin and FKBP-Shot-FRBEGFP with (maroon) and without (cyan) perfusion of 500 nM rapamycin. (H) There was a statistically significant difference in the MOC for the fraction of FKBP-Shot-FRBEGFP overlapping mCherry-Vinculin following the perfusion of 500 nM rapamycin (*p* value = 0.0101, Student's *t* test, *n* = 5–8 cells). (I) There was no statistically significant difference in the MOC for the fraction of mCherry-Vinculin overlapping with FKBP-Shot-FRBEGFP between cells perfused with 500 nM rapamycin and those not treated (*n* = 5–8 cells).

Shot's intramolecular conformation also regulates focal adhesion dynamics

Our FKBP-Shot-FRB-EGFP construct gives us the unique opportunity to test whether Shot's conformation plays a role in focal adhesion dynamics. We treated D25 cells with Shot RNAi, then transiently expressed both FKBP-Shot-FRB-EGFP and mCherry-Vinculin, and then tracked focal adhesion assembly and disassembly dynamics (Figure 8, A and B). Upon treatment with rapamycin, we observed a statistically significant increase in both focal adhesion assembly and disassembly (*p* = 0.0024 and 0.0001, respectively, Student's *t* test),

suggesting that when Shot is trapped in the "closed" confirmation, focal adhesion lifetimes are substantially reduced (Figure 8, C and D). Importantly, treatment of cells expressing mCherry-Vinculin alone following perfusion of rapamycin did not alter focal adhesion dynamics as there was no statistically significant difference in either focal adhesion assembly or disassembly between treated and untreated cells by our measurements (Figure 8, E and F). We also did not observe any differences in focal adhesion distribution or size when we compared cells with Shot in the "open" conformation (without rapamycin treatment) and those with Shot in the "closed"

conformation, following rapamycin perfusion (Supplemental Figure 3, C, D, and F). It was previously reported that the actin–microtubule cross-linking activity of Shot's mammalian homologue, ACF7, was insufficient to rescue the migration defects caused by its conditional knockout (Wu et al., 2008). Given that Shot is unable to cross-link actin and microtubules in the "closed" conformation (Applewhite et al., 2013), these results also suggest the actin–microtubule cross-linking is critical in Shot's role in regulating cell–matrix adhesion.

Depletion of Shot increases collective cell migration in vivo

Our results from tissue culture cells demonstrate that RNAi depletion of Shot leads to an increase in cell migration. We next wanted to determine whether this phenomenon can be observed in vivo. To do so, we tested Shot's role in migration during border cell migration, an in vivo model for collective cell migration. Drosophila border cell migration is a highly stereotypical developmental process that occurs during the maturation of oocytes. A group of six to 10 cells from the follicular epithelium that surrounds the oocyte and the supporting nurse cells delaminate and crawl through the nurse cells to the nurse cell/oocyte border, a distance of approximately 100 μm. This process is initiated at stage 9 of oocyte development and is completed by stage 10 (Montell, 2003). Using the UAS/GAL4 system, we are able to deplete Shot specifically in border cells using a hairpin RNAi flyline (UAS-Shot RNAi) (Subramanian et al., 2003), crossed with two different border cell–specific drivers, slbo-GAL4 and c306-GAL4 (Montell et al., 1992; Barth et al., 2012). To quantify the migration, we used the development of the egg chamber as a molecular clock and compared the distance the border cells migrated to the overall size of the oocyte and egg chamber, which increases with age. We took the ratio of oocyte area to egg chamber area to get a measurement of the relative "age" of the egg chamber and compared that to the ratio of the distance border cells traveled to their theoretical path to get their relative position in the egg chamber. Furthermore, we limited our measurements to stage 9 egg chambers (Szafranski and Goode, 2004) (Figure 9A). Despite being a highly stereotypical process, there is still some degree of heterogeneity during border cell migration, including exactly when and how many border cells delaminate during stage 9 and how fast they migrate (Bianco et al., 2007; Prasad and Montell, 2007; Prasad et al., 2007; Peercy and Starz-Gaiano, 2020). As such, we binned the position of the border cells (the ratio of actual migration length to theoretical length had they completed their journey) into early, mid, and late "bins" based on the overall length of the egg chamber divided into thirds, with the first third of the egg chamber representing the early stage, the second third representing the mid stage, and the final third representing the late stage of border cell migration (Figure 9G).

We first crossed UAS-Shot RNAi;;UAS-Dcr2 flies with a slbo-GAL4, which is balanced with a balancer chromosome that contains a curly (Cyo) wing marker (Figure 9, B and C). This cross resulted in 50% of the progeny inheriting the slbo-GAL4 driver and 50% of the progeny inheriting the balancer chromosome easily identified by curly wings in the adult. Egg chambers from these sibling flies served as an internal control. We then compared the position of the border cell cluster, binned into early, mid, and late stages, to the relative "age" of each egg chamber (Figure 9G). In the early (first third) stage of border cell migration, we did not observe any statistically significant differences between Shot-depleted border cells and their Cyo siblings. However, when we compared the mid (middle third) and late (final third) stages of border cell migration, we observed a statistically significant difference between Shot-depleted border cells and their Cyo siblings (p value < 0.0003, Student's t test for both bins) (Figure 9G). Thus, we consistently found that given the comparable

migration length distances, Shot-depleted border cells were younger than their Cyo sibling controls, suggesting that Shot border cells are migrating faster or delaminating from the surrounding follicular epithelium earlier than their Cyo siblings (Figure 9G). The slbo-GAL4 driver expresses during early stage 9 of newly delaminated border cells; however, c306-GAL4, which is an early anterior follicle cell driver, is also expressed at high levels in border cells and polar cells and begins driving expression at stages 4/5 of oocyte development (Aranjuez et al., 2012; Chen et al., 2020). We used this driver to deplete Shot during these earlier stages by crossing c306-GAL4 flies with either UAS-Shot RNAi;;UAS-Dcr2, UAS-Dcr2 alone as a control, or UAS-Arp3 RNAi flies and again binned the migration of the border cells into early, mid, and late periods of migration (Figure 9, D–F). Unlike our observations to form our slbo-GAL4 crosses, we observed statistically significant differences between control and Shot-depleted borders cells in all three of our bins (p value < 0.004, 0.002, and 0.012, Student's t test, respectively) (Figure 9H). Furthermore, border cells depleted of Arp3 trended in the opposite direction and were older than control egg chambers, suggesting slower migration, which is what would be expected for this condition (p value < 0.05 for mid-stage and p value < 0.0002 for late-stage migration, Student's t test) (Figure 9, F and H). While not the major contributor to border cell migration, integrins localize to cell–cell contacts in border cells and are required for proper border cell migration (Dinkins et al., 2008; Llense and Martín-Blanco, 2008). Thus, depletion of Shot, which increases focal adhesion dynamics in Drosophila tissue culture cells, may either lead to an increase in the dynamics of focal adhesion proteins during border cell migration, leading to faster migration, or weaken the adhesion between the border cells and the follicular epithelial, leading to precocious delamination. Collectively, results from our border cell migration assay corroborate our findings in tissue culture cells and suggest that depletion of Shot leads to altered cell–matrix adhesion both in cells and in vivo.

DISCUSSION

The role of spectraplakins during cell migration has been heavily scrutinized, and we have gleaned a great deal from work in mice. Loss of MACF1/ACF7 in several different mouse models not only decreases the rate of cell migration but also leads to less directional migration both in tissue culture cells and in vivo (Kodama et al., 2003; Wu et al., 2011; Ka et al., 2014; Ning et al., 2016; Yue et al., 2016). For example, conditional knockout studies of ACF7 carried out in mouse keratinocytes and endodermal cells revealed that when challenged with a wound these cells showed a delay in closure (Kodama et al., 2003; Wu et al., 2008; Yue et al., 2016). The same trend was also observed in myoblasts depleted of the two major isoforms of BPAG1, BPAG1a and BPAG1b (Guo et al., 1995; Poliakova et al., 2014). This decrease in cell migration also corresponded to an increase in focal adhesion size and a decrease in focal adhesion dynamics (Kodama et al., 2003; Wu et al., 2011; Yue et al., 2016).Thus, the findings we present here, that depletion of Shot leads to an increase in cell migration in several different cell lines (Figures 3 and 4) and in vivo (Figure 9), is somewhat surprising.

Michael and colleagues (2014) found that keratinocytes isolated from dystonin patients where BPAG1e is the dominant spectraplakin showed an increase in cell migration. There was a drastic reduction in BPAG1e expression in these cells, and this increase in migration speed was concomitant with a decrease in overall adhesion and a switch from cell β4 integrins as the primary cell–matrix receptor to β1 integrins. It is important to note that increased focal adhesion dynamics has been associated with increased rates of cell migration in mammalian tissue culture cells in other studies as
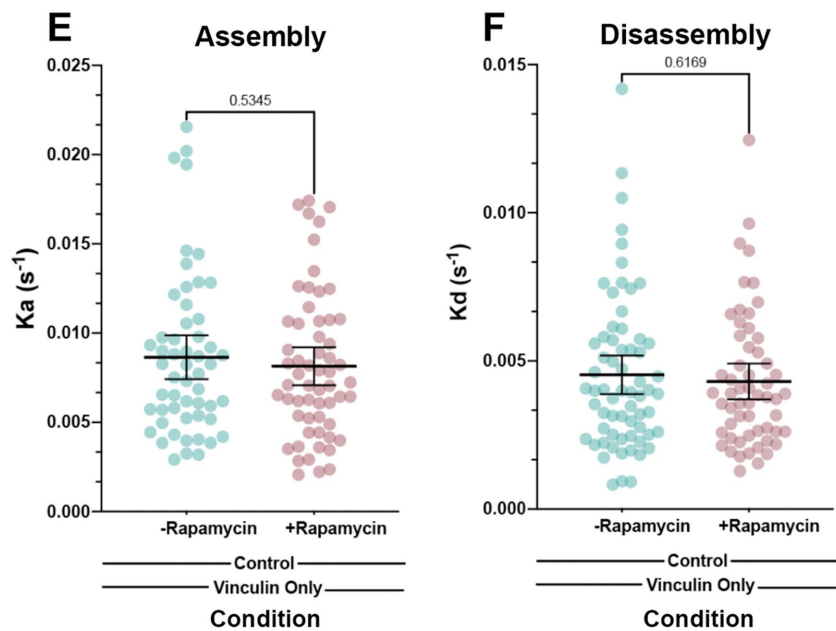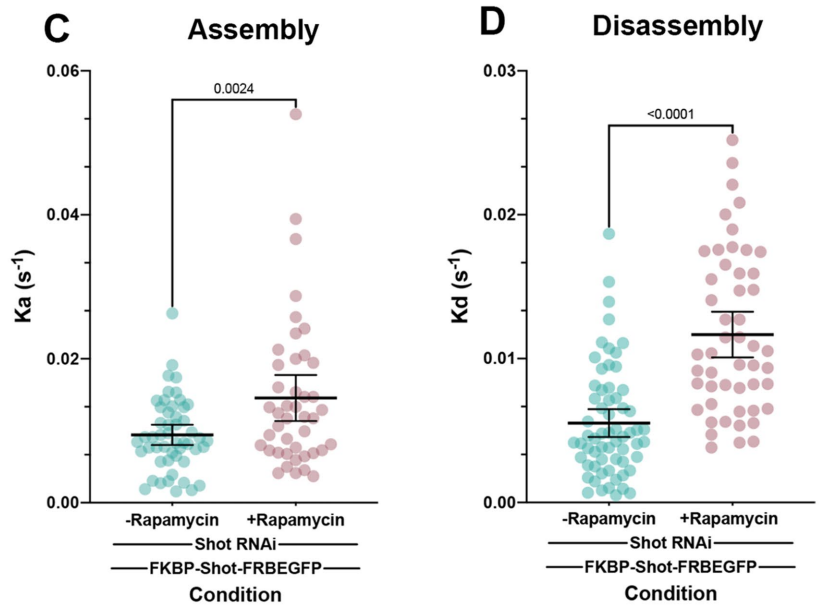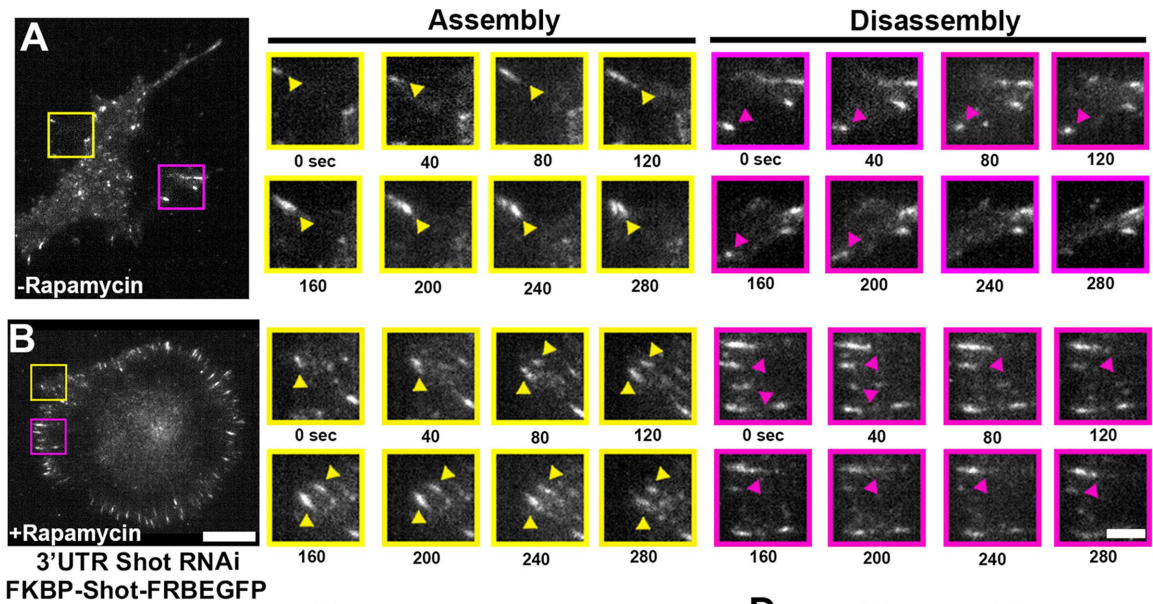
well (Laukaitis *et al.*, 2001; Webb *et al.*, 2004; Hu *et al.*, 2015). Reminiscent of these findings, our results indicate that depletion of Shot increases both the rate of focal adhesion assembly and disassembly, likely decreasing overall adhesion to the extracellular matrix (Figure 6). Thus, it appears that spectraplakins have differential effects on cell adhesion, leading to either an increase in adhesion and a corresponding decrease in cell migration as is the case with ACF7 or a decrease in adhesion and a corresponding increase in cell migration as is the case with cells isolated from dystonin patients or depletion of Shot. There are other similarities between keratinocytes isolated from dystonin patients and the *Drosophila*-derived tissue culture cells used in this study, namely that they are both acentrosomal in nature and that they predominantly express a single spectraplakin family member. Thus, it is possible that the shared phenotypes observed between these two systems could be rooted in these shared characteristics. To the latter point, the *Drosophila* tissue culture system is attractive as flies express a single spectraplakin family member, and while this protein family exhibits tissue-specific expression patterns and splice variants (Suozzi *et al.*, 2012; Voelzmann *et al.*, 2017), there is less potential for redundancy compared with other model systems. Furthermore, the dsRNA used in this study is shared by most Shot splice variants and thus we are likely decreasing the probability of redundancy. Also, given that *Drosophila* lacks cytoplasmic intermediate filaments (Adams *et al.*, 2000), we are also able to better isolate the role of actin–microtubule cross-linking during migration and eliminate the possible confounding factors of intermediate filament–based adhesion.

It has become increasingly clear that another important function of spectraplakins is organizing microtubule polarity in acentrosomal or noncentrosomal microtubule arrays (Nashchekin *et al.*, 2016; Ning *et al.*, 2016; Tillery *et al.*, 2018; Sun *et al.*, 2019; Lu *et al.*, 2021). This role in maintaining microtubule polarity may be critical given the role microtubules play in directing cell migration, mainly through signaling to the Rho family of GTPases (Waterman-Storer *et al.*, 1999; Rooney *et al.*, 2010). We observed a loss of microtubule polarity upon Shot depletion (Figure 5), a phenomenon reported by others (Wu *et al.*, 2008, 2011; Alves-Silva *et al.*, 2012; Kodama *et al.*, 2003), but despite this loss in polarity, we observed an increase in cell migration. This potential loss of spatial-temporal control of Rho family GTPases could also be a contributing factor to the aberrant migration that we observed in this study and represents an intriguing topic for future investigations.

While this may be the first study to explore the relationship between Shot and focal adhesion dynamics in *Drosophila*-derived tissue culture cells, Shot has long been associated with cell–matrix adhesion in studies carried out in vivo. In tendon cells, specialized cells that connect the cuticles of flies to the underlying muscle, Shot is thought to mechanically couple integrin-based junctions to the rest of the cytoskeleton (Strumpf and Volk, 1998; Subramanian *et al.*, 2003). Without Shot, the force of muscle contractions lead to rapture or separation of muscle from cuticle (Strumpf and Volk, 1998; Subramanian *et al.*, 2003; Hahn *et al.*, 2016). Shot was also uncovered in two independent screens for genes that cause wing blisters, a phenotype strongly associated with mutations to position specific (PS) integrin subunits (Prout *et al.*, 1997; Walsh and Brown, 1998). Beyond tendon cells, Shot also colocalizes with PS integrins at sites of epidermal attachment in developing embryos (Gregory and Brown, 1998). In light of the increased focal adhesion dynamics that we observed in migrating fly cells, Shot may function to stabilize integrin-based adhesions in general, and in its absence, focal adhesions are weaker and more dynamic. Furthermore, our results suggest that Shot's role in regulating focal adhesion dynamics is dependent on its ability to cross-link actin and microtubules (Applewhite *et al.*, 2013). Shot, when locked in "closed," cross-linking–inhibited conformation, showed decreased localization to focal adhesions and was unable to rescue the increased rates of focal adhesion assembly and disassembly that we observed upon Shot depletion (Figures 7 and 8). Alves-Silva and colleagues (2012) performed a series of tendon cell rescue experiments and also found that proper tendon cell adhesion could be achieved only by expression of Shot constructs that could functionally cross-link actin and microtubules, further suggesting that actin–microtubule cross-linking is important to Shot's role in regulating cell–matrix adhesion.

Cell–matrix adhesions not only chemically signal to the lamellipodia through molecules such as focal adhesion kinase (FAK) and the Rho family GTPases Rac and Rho, but they also mechanically signal to the lamellipodia through mechnosenitive molecules such as Vinculin and Talin (Jansen *et al.*, 2017). There is also a physical coupling of cell–matrix adhesions to the extracellular matrix, and in the event of weaker adhesion such as the case in Shot-depleted cells, the lamellipodia is less stable, leading to an increase in its dynamics as it probes the extracellular space (Galbraith *et al.*, 2007; Petrie *et al.*, 2009). Indicative of this, Shot depletion led to an overall increase in peripheral dynamics (Supplemental Figure 1) and an increase in the amplitude of lamellipodia protrusions as well as the speed of retraction (Figure 4). These results mirror that of FAK knockout (KO) fibroblasts, in that loss of FAK also led to a global increase in cell ruffling and peripheral dynamics (Swaminathan *et al.*, 2016). Upon closer examination of the lamellipodia of FAK-KO fibroblasts, there were

---

FIGURE 8: Shot's intramolecular conformation regulates focal adhesion assembly and disassembly dynamics. (A, B) *Drosophila* D25 cells coexpressing mCherry-Vinculin and FKBP-Shot-FRBEGFP following treatment with 3'UTR Shot RNAi. (A) Focal adhesion assembly (yellow box in low-magnification image) and disassembly (magenta box in low-magnification image) were tracked over time (right, marked by yellow and magenta borders, respectively) in the absence of rapamycin. Yellow and magenta arrows indicate individual focal adhesion assembly and disassembly events. (B) Focal adhesion assembly (yellow box in low-magnification image) and disassembly (magenta box in low-magnification image) were tracked over time (right, marked by yellow and magenta borders, respectively) following the addition of 500 nM rapamycin. Yellow and magenta arrows indicate individual focal adhesion assembly and disassembly dynamics, respectively. Scale bars 10 μm in low-magnification images and 2 μm in high-magnification images. (C–F) Scatter plots of the focal adhesion assembly (K_a) and disassembly (K_d) rate constants in the absence of rapamycin (cyan) and following perfusion with 500 nM rapamycin (red). (C) In cells expressing FKBP-Shot-FRBEGFP, the perfusion of 500 nM rapamycin led to a statistically significant increase in focal adhesion assembly (p value = 0.0024, Student's t test, 3–4 cells per condition, 43–51 individual focal adhesions). (D) In cells expressing FKBP-Shot-FRBEGFP, the perfusion of rapamycin led to a statistically significant increase in the rate of focal adhesion disassembly (p value < 0.0001, Student's t test, 3–4 cells per condition, 50–63 individual focal adhesions). (E, F) Perfusion of rapamycin does not alter focal adhesion assembly (4–5 cells, 54–59 individual focal adhesions) or disassembly (4–5 cells, 57–65 individual focal adhesions) dynamics.
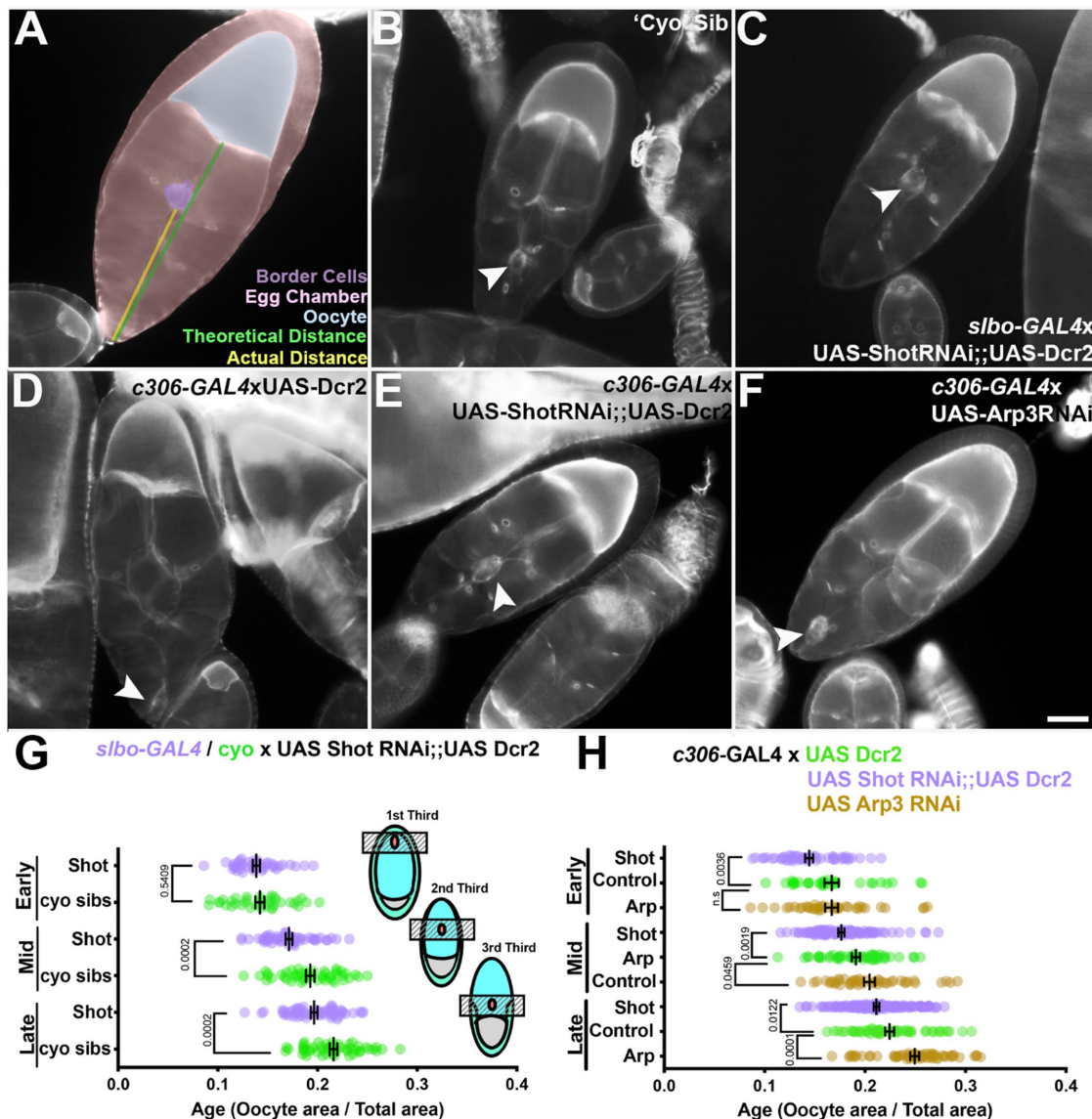
FIGURE 9: Depletion of Shot increases collective cell migration in vivo. (A) Diagram outlining how we derived the border cell migration index. We took the ratio of the size of the egg chamber (pink) and compared that to the size of the oocyte (blue) to get an approximate "age" of the egg chamber. We took the ratio of the distance the border cells migrated (yellow) to the distance of their theoretical path (green) to correlate the "age" of the egg chambers with how far the border cells (in purple) migrated. Border cells migrate from the tip of the egg chamber to the border of the oocyte. (B–F) Stage 9 border cells fixed and stained with phalloidin; white arrowheads indicate border cell clusters. (B, C) Egg chambers from *slbo-GAL4* driver x UAS-ShotRNAi;;UAS-Dcr2 cross. (B) "Cyo-Sibs" that did not inherit the *slbo-GAL4* driver and are controls. (C) *Slbo-GAL4* driver x UAS-ShotRNAi;;UAS-Dcr2 border cell clusters are depleted of Shot. (D–F) *c306-GAL4* flies crossed with (D) UAS-Dcr2, which served as controls, (E) UAS-ShotRNAi;;UAS-Dcr2, where Shot was depleted in border cell clusters, and (F) UAS-Arp3RNAi, where the Arp3 subunit was depleted in border cell clusters. Scale bar 20 µm. (G) Scatter plot of the migration index from the *slbo-GAL4* x UAS-ShotRNAi;;UAS-Dcr2 cross. "Cyo-Sibs" are shown in green circles, and Shot RNAi border cell clusters are in purple. (Right) The data were binned into early, mid, and late stages of border cell migration based on the length of the stage 9 egg chambers, where the bins represent the first, middle, and last third of the egg chamber. While there was no statistically significant difference between control and Shot-depleted border cells in the early bin, there was a statistically significant difference in our migration index in the mid (*p* value = 0.0002, Student's *t* test, N = 3, 47–49 egg chambers) and late (*p* value = 0.0002, Student's *t* test, N = 3, 49–58 egg chambers) stages or border cell migration. (H) Scatter plot of the migration index from the *c306-GAL4* cross to UAS-ShotRNAi;;UAS-Dcr2 (Shot, purple circles), UAS-Dcr2 (control, green), and UAS-Arp3RNAi (Arp, brown). The data were binned into early, mid, and late stages of border cell migration, and there was a statistically significant difference between control and Shot-depleted border cells in all three bins (*p* value = 0.0036, 0.0019, and 0.0122, respectively, Student's *t* test, N = 3, 31–124 egg chambers). Additionally, while was no statistically significant difference between control and Arp3-depleted border cells in the early bin, there was a statistically significant difference during the mid (*p* value = 0.0459, Student's *t* test, N = 3, 46–52 egg chambers) and late (*p* value = 0.0001, Student's *t* test, N = 3, 55–60 egg chambers) bins of border cell migration.

also significant increases in protrusion distance and retraction speeds (Swaminathan *et al.*, 2016). Thus, not only is Shot potentially involved in physical coupling of cell–matrix adhesions to the extracellular environment, but depletion of Shot may also interfere with the chemical signaling that occurs from adhesions.

Our analysis of Shot's role in border cell migration paints a picture similar to that observed when Shot-depleted border cells either migrated faster than controls or delaminated precociously from the surrounding follicular epithelium (Figure 9). Unfortunately, the analysis presented here cannot distinguish between these two possibilities; however, our results indicate a role for Shot in regulating adhesion that corroborates our results from *Drosophila* tissue culture cells. While not being a major contributor to border cell migration, depletion of integrins specifically in border cells does lead to a delay in migration (Dinkins *et al.*, 2008). Moreover, border cell migration is dependent on E-cadherin and cell–cell adhesion (Montell *et al.*, 2012; Cai *et al.*, 2014). Given that cell–cell and cell–matrix adhesions share many molecular components, are connected to the cytoskeleton in a similar manner, and are mechanically interdependent, the border cell migration phenotype that we observed could be the result of increased cell–cell adhesion dynamics brought upon by Shot depletion (Maruthamuthu *et al.*, 2011; Canel *et al.*, 2013; Mui *et al.*, 2016; De Pascalis and Etienne-Manneville, 2017). Indeed, clones of an amorphic allele of *shot*3 in the follicular epithelium led to a double-layering phenotype as well as an aberrant accumulation of actin and ZO-1. A slight reduction in Armadillo levels in some clones was also observed (Röper and Brown, 2003). Collectively, these results suggest that loss of Shot affects the integrity of the follicular epithelium, which gives rise to border cells. These changes in epithelia integrity brought up by the loss of Shot could be an indicator of a change in adhesion dynamics, which could translate to changes in the timing of border cell delamination or migration.

Conclusion

Depletion of Shot in fly cells leads to an increase in migration speeds that is likely the result of an increase in cell–matrix adhesion dynamics. Our results also indicate that Shot's cross-linking activity is needed for the regulation of focal adhesion dynamics as a Shot construct locked in a "closed" conformation was unable to rescue the increased focal adhesion dynamics that we observed upon Shot depletion. These increased adhesion dynamics may have contributed to the increase in border cell migration that we also observed.

MATERIALS AND METHODS
Request a protocol through *Bio-protocol*.

Cell culture
For a detailed description of *Drosophila* cell culturing, see Rogers and Rogers (2008), Currie and Rogers (2011), and Applewhite *et al.* (2016). All *Drosophila* cells were maintained in an incubator at 25°C. *Drosophila* ML-DmD17-c3, ML-DmD25c2, and Ras^{V12};*wts*^{RNAi} (DGRC, Bloomington, IN) were maintained in Schneider's media (Thermo Fisher Scientific, Waltham, MA) supplemented with 100× antibiotic–antimycotic (Thermo Fisher Scientific, Waltham, MA), 10% fetal bovine serum (FBS; Thermo Fisher Scientific, Waltham, MA), and 10 μg/ml insulin (Thermo Fisher Scientific, Waltham, MA). For detailed instructions on how to obtain dsRNA suitable for insect culture, see Rogers and Rogers (2008). Cells were incubated with 1 μl of dsRNA in 1 ml of cell culture media in six-well plates at 25°C for 24 h. Media and dsRNA were aspirated off and replenished each day of treatment for 7 d. dsRNA targets used in this article were previously characterized in Applewhite *et al.* (2010). The primers used to generate the

Shot and 3'UTR Shot dsRNA are as follows: Shot forward, 3'UTR Shot forward, 5'-TAATACGACTCACTATAGGggcaccagcaccattacccg-3' and 3'UTR reverse, 5'-TAATACGACTCACTATAGGggctacattcattgctaatgta-3', where the T7 promoter (needed to make dsRNA) is given in all uppercase letters. This generates a dsRNA template 440 base pairs long encompassing the final 267 nucleotides of Shot's coding sequence and 173 nucleotides of the 3'UTR of Shot. This region is shared by Shot variants A–C, E, G–Q, X, Z, and AA–AD as determined by a BLAST search. The primers used to generate RNAi against Rac1/2 are as follows: Rac1/2 fwd 5'-TAATACGACTCAC-TATAGGcacaaaacgcgagttaaagagg-3' and Rac1/2 rev 5'-TAATAC-GACTCACTATAGGcgagcactccagatacttgacc-3'. This specific RNAi template targets both Rac1 and Rac2 simultaneously. The primers used to generate RNAi against Mtl are as follows: Mtl fwd 5'-TAATA-CGACTCACTATAGGggcgaagtatagagattcctcgg-3' and Mtl rev 5'-TAA-TACGACTCACTATAGGctaggaaatgcatagatgctcg-3', where the T7 promoter is given in uppercase letters. Both Rac1/2 and Mtl dsRNAs were first characterized in Rogers *et al.* (2003).

Immunofluorescence and live-cell imaging
Cells were prepared for immunofluorescence and live-cell imaging as described in Applewhite *et al.* (2016). Briefly, ML-DmD17c3, ML-DmD25c2, and Ras^{V12};*wts*^{RNAi} cells were plated on glass-bottom dishes (1.5 glass coverslips attached to laser-cut 35-mm tissue culture dishes with UV-curable adhesive (Norland Products, Cranbury, NJ)) treated with ECM harvested from the cells as described in Currie and Rogers (2011). Cells were plated in Schneider's media supplemented with 100× antibiotic–antimycotic, 10% FBS, and 10 μg/ml insulin for both fixed and live-cell imaging. All transfections were carried out using FuGENE HD (Promega, Madison, WI). The expression of pMT vectors (Thermo Fisher Scientific, Waltham, MA) was achieved with 250–500 μM final concentration of copper sulfate unless noted otherwise. Cells were fixed using a 10% solution of paraformaldehyde (Electron Microscopy Sciences, Hatfield, PA) and PEM buffer (100 mM Pipes, 1 mM EGTA (ethylene glycol-bis(2-aminoethylether)-*N,N,N',N'*-tetraacetic acid), 1 mM MgCl$_2$). βPS antibody (Developmental Hybridoma Bank, Iowa City, IA) was diluted 1:200 in a 5% solution of normal goat serum (Sigma-Aldrich) and phosphate-buffered solution with 0.1% Triton X-100 (PBST) (Sigma-Aldrich). Secondary antibodies (Alexa 594; Jackson ImmunoResearch, West Grove, PA) and phalloidin (Alexa-488 and Alexa-594; Thermo Fisher Scientific) were used at a final dilution of 1:100 in PBST. Fixed cells were mounted using Dako antifade mounting media (Agilent, Santa Clara, CA). All imaging was performed on a TIRF system mounted on an inverted microscope (Ti-E; Nikon, Tokyo, Japan) using a 100×/1.49NA oil immersion TIRF objective driven by Nikon Elements software unless noted otherwise. Images were captured using an Orca-Flash 4.0 (Hamamatsu, Hamamatsu, Japan) and were processed for brightness and contrast using ImageJ before analysis.

Random cell migration assay and kymography
ML-DmD17-c3 and ML-DmD25c2 cells were plated at a subconfluent density on ECM-coated glass-bottom dishes and allowed to attach overnight. Cells were imaged every 5 min for 6 h by phase-contrast microscopy using a 40×/0.75NA objective. Individual cells were manually tracked using Manual Tracker (ImageJ). Cell directionality was calculated as a ratio of the direct distance between start and end points (D) to the total path length taken by the cells (T). To measure the rates of lamellipodial protrusion, retraction, persistence, frequency, and amplitude, kymographs were made using the Multi Kymograph ImageJ plug-in from phase-contrast movies

acquired every 2 s for 10 min. Kymographs were generated from phase-contrast movies of migrating D25 cells acquired every 2 s for 10 min. A line approximately 16 microns in width was drawn from the center of the cell to a few microns beyond the cell periphery. Following the protocol established by Hinz et al. (1999), these kymographs were used to extract the lamellipodial protrusion parameters. Statistics were performed using GraphPad Prism 7.

Quantification of peripheral dynamics

ML-DmD25c2 cells were transfected with EGFP-actin and plated on either ECM-coated glass-bottom dishes or con A–coated glass-bottom dishes and were imaged via TIRF microscopy using a 100X/1.49NA TIRF oil immersion objective and a 488 nm laser. Images were acquired every 3 s for a total of 5 min. All image processing was performed using ImageJ. For quantification, TIRF images were converted to binary and then the Find Edges plug-in was used to isolate the cell periphery. In some cases the Fill Holes plug-in was used to ensure continuity of the cell periphery. Next, a Max projection of the image series was generated. The resulting area (which would be greater for highly dynamic cell peripheries) was quantified. Graphs were made and statistics were performed using GraphPad Prism 7.

Colocalization analysis

Colocalization was analyzed by line-scan analysis and Mander's coefficient analysis. For line-scan analysis, a 10 μm line was drawn from the cell edge inward and fluorescence intensity was measured. These values were normalized and then averaged for all cells within that condition. Mander's coefficient analysis was performed using the Just Another Colocalization Program (JACoP) plug-in for ImageJ (Bolte and Cordelières, 2006). Briefly, intensity thresholds were manually set for both fluorescence channels and then the fraction of overlap was calculated in each direction. Images were captured by TIRF microscopy (described above).

Scratch-wound assays

Cells were plated on ECM-coated glass-bottom plates, and once attached, a scratch was drawn in the single-layer cell surface with a silicone-tipped metal syringe. The wells were then coated with oil to prevent evaporation and imaged every 5 min for 12–16 h under phase-contrast microscopy using a 40×/0.75NA objective. The scratch-wound assays were quantified by measuring the change in the area of the wound over time and by tracking single cells, both using FIJI. For microtubule polarity analysis, $Ras^{V12};wts^{RNAi}$ cells transfected with mRFP-tagged EB1 were plated on glass-bottom dishes coated with ECM etched in a similar manner. Cells were allowed to migrate 1 h before imaging. Images were captured by TIRF microscopy (described above) using a 100×/1.49NA oil immersion TIRF objective.

Quantification of focal adhesion assembly and disassembly rates

ML-DmD25c2 cells were transfected with mCherry-Vinculin (Ribeiro et al., 2014) under the control of the metallothionein promoter, which served as a marker for focal adhesions, and then imaged every 5 s over a 15-min period. The image analysis software Imaris (Bitplane, Concord, MA) was used to measure the intensity of the focal adhesions over time. The fluorescence of an area close to the focal adhesion was measured and subtracted from the focal adhesion fluorescence values in order to account for background fluorescence. To smooth out variation between different frames, a running three-frame average was applied to the fluorescence values of each frame (Stehbens et al., 2014). These values were then fitted against known

equations for assembly and disassembly, with disassembly modeled using single exponential decay and assembly represented as a sigmoid, logistic function (Stehbens et al., 2014). The assembly (K_a) and disassembly (K_d) constants for graphs that accurately represented changes in fluorescence values over time were then recorded. To corroborate that the values were not artifacts of background fluorescence, the sizes of the fluorescent objects were recorded and any object that was either smaller or larger than conventionally accepted focal adhesion measurements (0.5–10 μm^2) was discarded. Images were captured by TIRF microscopy (described above).

Border cell migration

Flies were raised on standard yeast/cornmeal agar at 25°C. One day before dissection, flies were fed yeast paste. Ovaries were then extracted from 6–8 flies per each condition per slide and fixed in a 10% solution of paraformaldehyde (Electron Microscopy Sciences, Hatfield, PA) and phosphate-buffered solution for ~30 min. They were then stained with Alexa568-phalloidin (Jackson ImmunoResearch, West Grove, PA) diluted 1:100 in PBST for at least 3 h at room temperature. Egg chambers were mounted on slides using Dako antifade mounting media (Agilent, Santa Clara, CA) and coverslips and sealed with clear nail polish. Slides were imaged by epifluorescence with a upright Leica DM400B microscope (Leica Microsystems, Buffalo Grove, IL) equipped with a Leica DFC425 C camera (Leica Microsystems, Buffalo Grove, IL) using 40×/0.65NA magnification. Egg chambers with border cells were staged and analyzed in FIJI. Quantification of border cell migration was carried out following the protocol established by Szafranski and Goode (2004). Flies used in this study were UAS-ShotRNAi;;UAS-Dcr2 (Subramanian et al., 2003), UAS-Dcr2, slbo-GAL4, c306-GAL4 (Bloomington Drosophila Resource Center, Bloomington, IN), and UAS-Arp3RNAi (108951/KK; Vienna Drosophila Resource Center, Vienna, Austria).

REFERENCES

Adams MD, Celniker SE, Holt RA, Evans CA, Gocayne JD, Amanatides PG, Scherer SE, Li PW, Hoskins RA, Galle RF, et al. (2000). The genome sequence of Drosophila melanogaster. Science 287, 2185–2195.

Alves-Silva J, Alves-Silva J, Sánchez-Soriano N, Beaven R, Klein M, Parkin J, Millard TH, Bellen HJ, Venken KJ, Ballestrem C, et al. (2012). Spectraplakins promote microtubule-mediated axonal growth by functioning as structural microtubule-associated proteins and EB1-dependent + TIPs (tip interacting proteins). J Neurosci 32, 9143–9158.

Applewhite DA, Davis CA, Griffis ER, Quintero OA (2016). Imaging of the cytoskeleton using live and fixed Drosophila tissue culture cells. In: Cytoskeleton Methods and Protocols, ed. RH Gavin, New York: Springer New York, 83–97.

Applewhite DA, Grode KD, Duncan MC, Rogers SL (2013). The actin-microtubule cross-linking activity of *Drosophila* Short stop is regulated by intramolecular inhibition. Mol Biol Cell 24, 2885–2893.

Applewhite DA, Grode KD, Keller D, Zadeh AD, Slep KC, Rogers SL (2010). The Spectraplakin Short Stop is an actin–microtubule cross-linker that contributes to organization of the microtubule network. Mol Biol Cell 21, 1714–1724.

Aranjuez G, Kudlaty E, Longworth MS, McDonald JA (2012). On the role of PDZ domain-encoding genes in Drosophila border cell migration. G3 GenesGenomesGenetics 2, 1379–1391.

Barth JM, Hafen E, Köhler K (2012). The lack of autophagy triggers precocious activation of Notch signaling during Drosophila oogenesis. BMC Dev Biol 12, 35.

Bear JE, Svitkina TM, Krause M, Schafer DA, Loureiro JJ, Strasser GA, Maly IV, Chaga OY, Cooper JA, Borisy GG, *et al.* (2002). Antagonism between Ena/VASP proteins and actin filament capping regulates fibroblast motility. Cell 109, 509–521.

Beningo KA, Dembo M, Kaverina I, Small JV, Wang Y (2001). Nascent focal adhesions are responsible for the generation of strong propulsive forces in migrating fibroblasts. J Cell Biol 153, 881–888.

Bernier G, Mathieu M, Repentigny YD, Vidal SM, Kothary R (1996). Cloning and characterization of mouse ACF7, a novel member of the dystonin subfamily of actin binding proteins. Genomics 38, 19–29.

Bianco A, Poukkula M, Cliffe A, Mathieu J, Luque CM, Fulga TA, Rørth P (2007). Two distinct modes of guidance signalling during collective migration of border cells. Nature 448, 362–365.

Bolte S, Cordelières FP (2006). A guided tour into subcellular colocalization analysis in light microscopy. J Microsc 224, 213–232.

Burridge K, Chrzanowska-Wodnicka M (1996). Focal adhesions, contractility, and signaling. Annu Rev Cell Dev Biol 12, 463–519.

Cai D, Chen S-C, Prasad M, He L, Wang X, Choesmel-Cadamuro V, Sawyer JK, Danuser G, Montell DJ (2014). Mechanical feedback through E-cadherin promotes direction sensing during collective cell migration. Cell 157, 1146–1159.

Canel M, Serrels A, Frame MC, Brunton VG (2013). E-cadherin–integrin crosstalk in cancer invasion and metastasis. J Cell Sci, jcs.100115.

Chen Y, Kotian N, Aranjuez G, Chen L, Messer CL, Burtscher A, Sawant K, Ramel D, Wang X, McDonald JA (2020). Protein phosphatase 1 activity controls a balance between collective and single cell modes of migration. eLife 9, e52979.

Cho A, Kato M, Whitwam T, Kim JH, Montell DJ (2016). An atypical tropomyosin in Drosophila with intermediate filament-like properties. Cell Rep 16, 928–938.

Choi H-J, Park-Snyder S, Pascoe LT, Green KJ, Weis WI (2002). Structures of two intermediate filament-binding fragments of desmoplakin reveal a unique repeat motif structure. Nat Struct Biol 9, 612–620.

Cramer LP (1999). Role of actin-filament disassembly in lamellipodium protrusion in motile cells revealed using the drug jasplakinolide. Curr Biol 9, 1095–1105.

Currie JD, Rogers SL (2011). Using the Drosophila melanogaster D17-c3 cell culture system to study cell motility. Nat Protoc 6, 1632–1641.

Delorme-Walker VD, Peterson JR, Chernoff J, Waterman CM, Danuser G, DerMardirossian C, Bokoch GM (2011). Pak1 regulates focal adhesion strength, myosin IIA distribution, and actin dynamics to optimize cell migration. J Cell Biol 193, 1289–1303.

De Pascalis C, Etienne-Manneville S (2017). Single and collective cell migration: the mechanics of adhesions. Mol Biol Cell 28, 1833–1846.

Dinkins MB, Fratto VM, LeMosy EK (2008). Integrin alpha chains exhibit distinct temporal and spatial localization patterns in epithelial cells of the *Drosophila* ovary. Dev Dyn 237, 3927–3939.

Dogterom M, Koenderink GH (2019). Actin–microtubule crosstalk in cell biology. Nat Rev Mol Cell Biol 20, 38–54.

Dunn KW, Kamocka MM, McDonald JH (2011). A practical guide to evaluating colocalization in biological microscopy. Am J Physiol Cell Physiol 300, C723–C742.

Galbraith CG, Yamada KM, Galbraith JA (2007). Polymerizing actin fibers position integrins primed to probe for adhesion sites. Science 315, 992–995.

Gally C, Zhang H, Labouesse M (2016). Functional and genetic analysis of VAB-10 spectraplakin in Caenorhabditis elegans. Methods Enzymol 569, 407–430.

Goryunov D, Liem RKH (2016). Microtubule-Actin Cross-Linking Factor 1: Domains, Interaction Partners, and Tissue-Specific Functions. Methods Enzymol 569, 331–353.

Gregory SL, Brown NH (1998). kakapo, a gene required for adhesion between and within cell layers in Drosophila, encodes a large cytoskeletal linker protein related to plectin and dystrophin. J Cell Biol 143, 1271–1282.

Grum VL, Li D, MacDonald RI, Mondragón A (1999). Structures of two repeats of spectrin suggest models of flexibility. Cell 98, 523–535.

Gundersen GG, Bulinski JC (1988). Selective stabilization of microtubules oriented toward the direction of cell migration. Proc Natl Acad Sci USA 85, 5946–5950.

Guo L, Degenstein L, Dowling J, Yu Q-C, Wollmann R, Perman B, Fuchs EG (1995). Gene targeting of BPAG1: abnormalities in mechanical strength and cell migration in stratified epithelia and neurologic degeneration. Cell 81, 233–243.

Gupton SL, Eisenmann K, Alberts AS, Waterman-Storer CM (2007). mDia2 regulates actin and focal adhesion dynamics and organization in the lamella for efficient epithelial cell migration. J Cell Sci 120, 3475–3487.

Gupton SL, Waterman-Storer CM (2006). Spatiotemporal feedback between actomyosin and focal-adhesion systems optimizes rapid cell migration. Cell 125, 1361–1374.

Hahn I, Ronshaugen M, Sánchez-Soriano N, Prokop A (2016). Functional and genetic analysis of spectraplakins in Drosophila. Methods Enzymol 569, 373–405.

Hinz B, Alt W, Johnen C, Herzog V, Kaiser H-W (1999). Quantifying lamella dynamics of cultured cells by SACED, a new computer-assisted motion analysis. Exp Cell Res 251, 234–243.

Honnappa S, Gouveia SM, Weisbrich A, Damberger FF, Bhavesh NS, Jawhari H, Grigoriev I, van Rijssel FJ, Buey RM, Lawera A, *et al.* (2009). An EB1-binding motif acts as a microtubule tip localization signal. Cell 138, 366–376.

Hu L, Su P, Li R, Yin C, Zhang Y, Shang P, Yang T, Qian A (2016). Isoforms, structures, and functions of versatile spectraplakin MACF1. BMB Rep 49, 37–44.

Hu Y, Lu J, Xu X, Lyu J, Zhang H (2017). Regulation of focal adhesion turnover in SDF-1α-stimulated migration of mesenchymal stem cells in neural differentiation. Sci Rep 7, 10013.

Hu Y-L, Lu S, Szeto KW, Sun J, Wang Y, Lasheras JC, Chien S (2015). FAK and paxillin dynamics at focal adhesions in the protrusions of migrating cells. Sci Rep 4, 6024.

Ivanova SI, Chakarov S, Momchilova A, Pankov R (2017). Live-cell biosensor for assessment of adhesion qualities of biomaterials. Mater Sci Eng C 78, 230–238.

Jansen KA, Atherton P, Ballestrem C (2017). Mechanotransduction at the cell-matrix interface. Semin Cell Dev Biol 71, 75–83.

Jefferson JJ, Leung CL, Liem RKH (2004). Plakins: Goliaths that link cell junctions and the cytoskeleton. Nat Rev Mol Cell Biol 5, 542–553.

Jefferson JJ, Leung CL, Liem RKH (2006). Dissecting the sequence specific functions of alternative N-terminal isoforms of mouse bullous pemphigoid antigen 1. Exp Cell Res 312, 2712–2725.

Ka M, Jung E-M, Mueller U, Kim W-Y (2014). MACF1 regulates the migration of pyramidal neurons via microtubule dynamics and GSK-3 signaling. Dev Biol 395, 4–18.

Kodama A, Karakesisoglou I, Wong E, Vaezi A, Fuchs E (2003). ACF7: an essential integrator of microtubule dynamics. Cell 115, 343–354.

Laukaitis CM, Webb DJ, Donais K, Horwitz AF (2001). Differential dynamics of α5 integrin, paxillin, and α-actinin during formation and disassembly of adhesions in migrating cells. J Cell Biol 153, 1427–1240.

Lawson CD, Burridge K (2014). The on-off relationship of Rho and Rac during integrin-mediated adhesion and cell migration. Small GTPases 5, e27958.

Llense F, Martín-Blanco E (2008). JNK signaling controls border cell cluster integrity and collective cell migration. Curr Biol 18, 538–544.

Lu W, Lakonishok M, Gelfand VI (2021). Gatekeeper function for Short stop at the ring canals of the Drosophila ovary. Curr Biol, S0960982221006692.

Machesky LM, Atkinson SJ, Ampe C, Vandekerckhove J, Pollard TD (1994). Purification of a cortical complex containing two unconventional actins from Acanthamoeba by affinity chromatography on profilin-agarose. J Cell Biol 127, 107–115.

Maruthamuthu V, Sabass B, Schwarz US, Gardel ML (2011). Cell-ECM traction force modulates endogenous tension at cell-cell contacts. Proc Natl Acad Sci USA 108, 4708–4713.

Mayor R, Etienne-Manneville S (2016). The front and rear of collective cell migration. Nat Rev Mol Cell Biol 17, 97–109.

Michael M, Begum R, Fong K, Pourreyrone C, South AP, McGrath JA, Parsons M (2014). BPAG1-e restricts keratinocyte migration through control of adhesion stability. J Invest Dermatol 134, 773–782.

Mirijanian DT, Chu J-W, Ayton GS, Voth GA (2007). Atomistic and coarse-grained analysis of double spectrin repeat units: the molecular origins of flexibility. J Mol Biol 365, 523–534.

Mitchison T, Kirschner M (1984). Dynamic instability of microtubule growth. Nature 312, 237–242.

Montell DJ (2003). Border-cell migration: the race is on. Nat Rev Mol Cell Biol 4, 13–24.

Montell DJ, Rorth P, Spradling AC (1992). Slow border cells, a locus required for a developmentally regulated cell migration during oogenesis, encodes Drosophila C/EBP. Cell 71, 51–62.

Montell DJ, Yoon WH, Starz-Gaiano M (2012). Group choreography: mechanisms orchestrating the collective movement of border cells. Nat Rev Mol Cell Biol 13, 631–645.

Mui KL, Chen CS, Assoian RK (2016). The mechanical regulation of integrin–cadherin crosstalk organizes cells, signaling and forces. J Cell Sci, jcs.183699.

Mullins RD, Heuser JA, Pollard TD (1998). The interaction of Arp2/3 complex with actin: nucleation, high affinity pointed end capping, and formation of branching networks of filaments. Proc Natl Acad Sci USA 95, 6181–6186.

Nashchekin D, Fernandes AR, St Johnston D (2016). Patronin/Shot cortical foci assemble the noncentrosomal microtubule array that specifies the Drosophila anterior-posterior axis. Dev Cell 38, 61–72.

Nayal A, Webb DJ, Brown CM, Schaefer EM, Vicente-Manzanares M, Horwitz AR (2006). Paxillin phosphorylation at Ser273 localizes a GIT1–PIX–PAK complex and regulates adhesion and protrusion dynamics. J Cell Biol 173, 587–589.

Ning W, Yu Y, Xu H, Liu X, Wang D, Wang J, Wang Y, Meng W (2016). The CAMSAP3-ACF7 complex couples noncentrosomal microtubules with actin filaments to coordinate their dynamics. Dev Cell 39, 61–74.

O'Connell ME, Sridharan D, Driscoll T, Krishnamurthy I, Perry WG, Applewhite DA (2019). The *Drosophila* protein, Nausicaa, regulates lamellipodial actin dynamics in a cortactin-dependent manner. Biol Open bio.038232.

Peercy BE, Starz-Gaiano M (2020). Clustered cell migration: modeling the model system of Drosophila border cells. Semin Cell Dev Biol 100, 167–176.

Petrie RJ, Doyle AD, Yamada KM (2009). Random versus directionally persistent cell migration. Nat Rev Mol Cell Biol 10, 538–549.

Poliakova K, Adebola A, Leung CL, Favre B, Liem RKH, Schepens I, Borradori L (2014). BPAG1a and b associate with EB1 and EB3 and modulate vesicular transport, Golgi apparatus structure, and cell migration in C2.7 myoblasts. PLoS ONE 9, e107535.

Ponti A (2004). Two distinct actin networks drive the protrusion of migrating cells. Science 305, 1782–1786.

Prasad M, Jang AC-C, Starz-Gaiano M, Melani M, Montell DJ (2007). A protocol for culturing Drosophila melanogaster stage 9 egg chambers for live imaging. Nat Protoc 2, 2467–2473.

Prasad M, Montell DJ (2007). Cellular and molecular mechanisms of border cell migration analyzed using time-lapse live-cell imaging. Dev Cell 12, 997–1005.

Prout M, Damania Z, Soong J, Fristrom D, Fristrom JW (1997). Autosomal mutations affecting adhesion between wing surfaces in *Drosophila melanogaster*. Genetics 146, 275–285.

Raftopoulou M, Hall A (2004). Cell migration: Rho GTPases lead the way. Dev Biol 265, 23–32.

Ribeiro SA, D'Ambrosio MV, Vale RD (2014). Induction of focal adhesions and motility in *Drosophila* S2 cells. Mol Biol Cell 25, 3861–3869.

Rogers GC, Rusan NM, Peifer M, Rogers SL (2008). A multicomponent assembly pathway contributes to the formation of acentrosomal microtubule arrays ininterphase *Drosophila* Cells. Mol Biol Cell 19, 3163–3178.

Rogers SL, Rogers GC (2008). Culture of Drosophila S2 cells and their use for RNAi-mediated loss-of-function studies and immunofluorescence microscopy. Nat Protoc 3, 606–611.

Rogers SL, Wiedemann U, Stuurman N, Vale RD (2003). Molecular requirements for actin-based lamella formation in Drosophila S2 cells. J Cell Biol 162, 1079–1088.

Rooney C, White G, Nazgiewicz A, Woodcock SA, Anderson KI, Ballestrem C, Malliri A (2010). The Rac activator STEF (Tiam2) regulates cell migration by microtubule-mediated focal adhesion disassembly. EMBO Rep 11, 292–298.

Röper K, Brown NH (2003). Maintaining epithelial integrity. J Cell Biol 162, 1305–1315.

Röper K, Gregory SL, Brown NH (2002). The "spectraplakins": cytoskeletal giants with characteristics of both spectrin and plakin families. J Cell Sci 115, 4215–4225.

Schratt G, Philippar U, Berger J, Schwarz H, Heidenreich O, Nordheim A (2002). Serum response factor is crucial for actin cytoskeletal organization and focal adhesion assembly in embryonic stem cells. J Cell Biol 156, 737–750.

Seetharaman S, Etienne-Manneville S (2020). Cytoskeletal crosstalk in cell migration. Trends Cell Biol 30, 720–735.

Simcox A, Mitra S, Truesdell S, Paul L, Chen T, Butchar JP, Justiniano S (2008). Efficient genetic method for establishing Drosophila cell lines unlocks the potential to create lines of specific genotypes. PLoS Genet 4, e1000142.

Slep KC, Rogers SL, Elliott SL, Ohkura H, Kolodziej PA, Vale RD (2005). Structural determinants for EB1-mediated recruitment of APC and spectraplakins to the microtubule plus end. J Cell Biol 168, 587–598.

Small JV, Resch GP (2005). The comings and goings of actin: coupling protrusion and retraction in cell motility. Curr Opin Cell Biol 17, 517–523.

Small JV, Stradal T, Vignal E, Rottner K (2002). The lamellipodium: where motility begins. Trends Cell Biol 12, 112–120.

Stehbens SJ, Paszek M, Pemble H, Ettinger A, Gierke S, Wittmann T (2014). CLASPs link focal-adhesion-associated microtubule capture to localized exocytosis and adhesion site turnover. Nat Cell Biol 16, 558–570.

Strumpf D, Volk T (1998). Kakapo, a novel cytoskeletal-associated protein is essential for the restricted localization of the neuregulin-like factor, Vein, at the muscle–endon junction site. J Cell Biol 143, 1259–1270.

Subramanian A, Prokop A, Yamamoto M, Sugimura K, Uemura T, Betschinger J, Knoblich JA, Volk T (2003). Shortstop recruits EB1/APC1 and promotes microtubule assembly at the muscle-tendon junction. Curr Biol 13, 1086–1095.

Sun T, Song Y, Dai J, Mao D, Ma M, Ni J-Q, Liang X, Pastor-Pareja JC (2019). Spectraplakin Shot maintains perinuclear microtubule organization in Drosophila polyploid cells. Dev Cell 49, 731–747.e7.

Suozzi KC, Wu X, Fuchs E (2012). Spectraplakins: master orchestrators of cytoskeletal dynamics. J Cell Biol 197, 465–475.

Svitkina TM, Borisy GG (1999). Arp2/3 complex and actin depolymerizing factor/cofilin in dendritic organization and treadmilling of actin filament array in lamellipodia. J Cell Biol 145, 1009–1026.

Swaminathan V, Fischer RS, Waterman CM (2016). The FAK–Arp2/3 interaction promotes leading edge advance and haptosensing by coupling nascent adhesions to lamellipodia actin. Mol Biol Cell 27, 1085–1100.

Szafranski P, Goode S (2004). A Fasciclin 2 morphogenetic switch organizes epithelial cell cluster polarity and motility. Development 131, 2023–2036.

Tillery M, Blake-Hedges C, Zheng Y, Buchwalter R, Megraw T (2018). Centrosomal and non-centrosomal microtubule-organizing centers (MTOCs) in Drosophila melanogaster. Cells 7, 121.

Ui K, Ueda R, Miyake T (1987). Cell lines from imaginal discs of Drosophila melanogaster. In Vitro Cell Dev Biol 23, 707–711.

Voelzmann A, Liew Y-T, Qu Y, Hahn I, Melero C, Sánchez-Soriano N, Prokop A (2017). Drosophila Short stop as a paradigm for the role and regulation of spectraplakins. Semin Cell Dev Biol 69, 40–57.

Walsh EP, Brown NH (1998). A screen to identify Drosophila genes required for integrin-mediated adhesion. Genetics 150, 791–805.

Wang F, Chen S, Liu HB, Parent CA, Coulombe PA (2018). Keratin 6 regulates collective keratinocyte migration by altering cell–cell and cell–matrix adhesion. J Cell Biol 217, 4314–4330.

Waterman-Storer CM, Salmon ED (1997). Actomyosin-based retrograde flow of microtubules in the lamella of migrating epithelial cells influences microtubule dynamic instability and turnover and is associated with microtubule breakage and treadmilling. J Cell Biol 139, 417–434.

Waterman-Storer CM, Worthylake RA, Liu BP, Burridge K, Salmon ED (1999). Microtubule growth activates Rac1 to promote lamellipodial protrusion in fibroblasts. Nat Cell Biol 1, 45–50.

Webb DJ, Donais K, Whitmore LA, Thomas SM, Turner CE, Parsons JT, Horwitz AF (2004). FAK–Src signalling through paxillin, ERK and MLCK regulates adhesion disassembly. Nat Cell Biol 6, 154–161.

Wu X, Kodama A, Fuchs E (2008). ACF7 regulates cytoskeletal-focal adhesion dynamics and migration and has ATPase activity. Cell 135, 137–148.

Wu X, Shen Q-T, Oristian DS, Lu CP, Zheng Q, Wang H-W, Fuchs E (2011). Skin stem cells orchestrate directional migration by regulating microtubule-ACF7 connections through GSK3β. Cell 144, 341–352.

Yue J, Zhang Y, Liang WG, Gou X, Lee P, Liu H, Lyu W, Tang WJ, Chen SY, Yang F, *et al.* (2016). In vivo epidermal migration requires focal adhesion targeting of ACF7. Nat Commun 7, 11692.